Implementing magnon-photon interaction using analytical and numerical techniques

by

Oluwanisola Jephthah Iyaro

A Thesis submitted to the Faculty of Graduate Studies of

The University of Manitoba

in partial fulfillment of the requirements for the degree of

Master of Science

Department of Physics and Astronomy

University of Manitoba

Winnipeg, Canada

Abstract

The interaction between magnons and photons has significant implications for quantum information processing and in spintronics. In an electromagnetic cavity, wherein photons are confined, the photon-magnon coupling can be enhanced and controlled more effectively. In this thesis, we investigate a model system wherein the interaction between an antiferromagnetic domain wall and cavity photons occurs via the inverse Faraday effect, resulting in a coupling analogous to optomechanical coupling. The coupled dynamics leads to the emergence of level attraction, a term used to describe the coalescence of two distinct eigenmodes in a region bounded by exceptional points. We reveal the impact of the Dzyaloshinskii-Moriya Interaction (DMI) on the coupled dynamics of domain walls to cavity photons. We demonstrate that the presence of DMI can affect the coupling between magnons and photons, depending on the geometry of the system. This finding has potential applications in the control and detection of DMI in antiferromagnetic materials. Using a different formalism, we provide a demonstration that the phenomenon of level attraction can arise in systems characterized by instability under non-equilibrium conditions. A formalism for characterizing the linear response of driven magnonic systems has been developed and we show that results can be reproduced using numerical micromagnetics. The developed theory facilitates the study of cavity magnonics using numerical micromagnetics.

Acknowledgements

I would like to express my sincere gratitude to my advisor, Prof. Stamps, for offering his genuine support and guidance throughout this academic journey. I am truly grateful for his patience, encouragement and advice, which are always wise, sound and practical. I also appreciate Profs. Jacob Burgess and Can-Ming Hu who played a significant role in the completion of this thesis. Many thanks go to Igor Proskurin for his unwavering support both as a colleague and a friend.

I appreciate Susan Beshta and Robyn Beaulieu for their invaluable administrative support. Their efficiency, responsiveness, and willingness to assist with various administrative tasks before my arrival in Canada and during my time at the department helped keep my studies on track. I extend my thanks to the department's information technologist, Maiko Langelaar for his prompt technical assistance and friendly chats. I would like to acknowledge Dr. Ruth Cameron and Andriy Yamchuk for their supervision during the period I served as a Teaching Assistant. Their guidance and knowledge have been instrumental in shaping my teaching skills and fostering a better ability to work with students taking physics.

To all the wonderful collegaues and friends I met during my time in Winnipeg, I want to express my heartfelt thanks. The memories we have created will always hold a special place in my heart. I must also express my gratitude to my family for their ever present support and understanding. Their encouragement have been a constant source of mental sustenance throughout this journey.

My appreciation also goes to the Natural Sciences and Engineering Research Council of Canada (NSERC) Discovery, John R. Leaders Fund - Canada Foundation for Innovation (CFI-JELF), Research Manitoba and the University of Manitoba, Canada for their financial support during the course of my studies.

Contribution of authors

This thesis is based on the work of a collaborative research group, leading to publications in references [1] and [2]. The details of contributions are as follows:

Chapter 2 is a product of a collaborative effort where Robert Stamps provided overall supervision and insightful intellectual guidance on all aspects of the study. Igor Proskurin actively engaged in discussions, meticulously reviewed and corrected the manuscript. The author of this thesis played a major role in performing the analytical calculations, producing the results, writing the original manuscript, and managing communications with journal referees, thereby ensuring the coherence and integrity of the work.

The formalism in Chapter 3 was developed by Igor Proskurin who was also the principal investigator in the formulation of the theoretical model and wrote the original manuscript. Robert Stamps offered invaluable insights, support and supervisory role throughout the project. The author of this thesis made substantial contributions to the software and performed the numerical calculations that produced the results presented, which are at the computational core of the work. More details about the author's contribution are below:

The author performed the micromagnetic simulations of the spin dynamics in Chapter 3 using the MuMax3 package [3], and by using the theoretical conditions for realizing a P-mode in Ref. [4], the author numerically searched for and identified the initial conditions that produced a stable P-mode in MuMax3. The author also introduced excitations around a stable P mode and numerically performed the derivatives which enter into the susceptibility equation. The data obtained by the author were used by Igor Proskurin to obtain the spectrum and density plots of the system's response.

The collective effort of the group, driven by the author's dedication has been instrumental in putting all the research together.

Bibliography

[1] Jephthah O. Iyaro, Igor Proskurin, and Robert L. Stamps. Collective dynamics of domain walls: An antiferromagnetic spin texture in an optical cavity. *Phys. Rev. B*, 104:184416, Nov 2021.

[2] Igor Proskurin, Jephthah O. Iyaro, and Robert L. Stamps. Mode attraction in floquet systems with memory: Application to magnonics. *Phys. Rev. B*, 105:224420, Jun 2022.

[3] Arne Vansteenkiste, Jonathan Leliaert, Mykola Dvornik, Mathias Helsen, Felipe Garcia-Sanchez, and Bartel Van Waeyenberge. The design and verification of MuMax3. *AIP Advances*, 4(10):107133, oct 2014.

[4] Giorgio Bertotti, Claudio Serpico, and Isaak D. Mayergoyz. Nonlinear magnetization dynamics under circularly polarized field. *Phys. Rev. Lett.*, 86:724–727, Jan 2001.

Contents

List of Figures v

1 Introduction 1

2 Collective dynamics of an antiferromagnetic domain wall in an optical cavity 9

2.1 The model . . . 11

2.2 Domain wall dynamics . . . 15

2.3 Conclusion . . . 20

3 Mode attraction in Floquet systems with memory: application to magnonics 29

3.1 Introduction . . . 29

3.2 General formalism . . . 32

3.2.1 Kinetic equation for the probe system . . . 33

3.2.2 Semi-classical periodically driven systems . . . 34

3.3 Application to magnonics . . . 35

3.3.1 Semi-classical spin driven by the circularly polarize magnetic field . . . 36

3.3.2 Level attraction with cavity photons outside of equilibrium . . . 39

3.4 Numerical results and discussion . . . 40

3.5 Conclusion . . . 41

4 Conclusions and future outlook 47

Appendices 49

A Domain wall configuration 50

B Dzyalonshinskii-Moriya interaction (DMI) **55**

C Master equation for open systems **58**

C.1 Formal solution for $\Delta\hat{\rho}(t)$ and master equation for $\hat{\rho}(t)$ 59

C.2 Kinetic equations for dynamic variables 60

D Perturbative expansion over a P-mode solution **64**

List of Figures

2.1 Domain wall with DMI along $\hat{y}$ interacting with cavity photons 12

2.2 Frequency gap dependence on the presence of DMI in the $\hat{y}$ direction 14

2.3 Domain wall with DMI along $\hat{y}$ interacting with cavity photons 15

2.4 Effect of DMI in the $\hat{y}$ direction on the frequency gap 19

3.1 Schematic of a magnetic specimen in a microwave resonator exhibiting a P-mode . . . 31

3.2 Response function showing two bands that correspond to excitations above a P-mode 38

Chapter 1

Introduction

The interaction between electromagnetic (EM) radiation and magnetic materials is an important topic in the field of condensed matter physics. While the principles of magnetism is an older subject, ferromagnetic resonance (FMR), a phenomenon that stems from the absorption of electromagnetic waves by magnetic materials only became a topic of discussion in the 20th century, leading to experimental observation by Griffiths [1]. Theoretical studies providing insights into how magnetic materials can be excited by EM fields resulted in the prediction of FMR, which explains how a magnetic material absorbs EM radiation when the precessional frequency of the magnetization in the material matches the frequency of the EM radiation. The theoretical explanation was first formulated by Landau and Lifshitz [2] to describe the dynamic behavior of ferromagnetic materials near resonance and has since then been modified to account for damping effects [3], demagnetization and anisotropy.

When EM radiation is absorbed by a ferromagnet, the resonant effect on a single spin can traverse the material via the exchange interaction between the spins, resulting in collective excitations called magnons. The coupling between magnons and photons then forms a new kind of quasi-particles called magnon-polaritons. Cavity resonators, which confine photons, are employed to increase the rate of production of these magnon-polaritons in the system and also improve the control and detection of magnon-photon coupling [4]. Due to the role an electromagnetic cavity plays, this kind of study is often referred to as cavity magnonics. Cavity magnonics, in a nutshell, is a field of research that investigates the interaction between magnons, the fundamental excitations in magnetically ordered

systems, and photons [5, 6]. This relatively new field of study has continued to attract a lot of attention in recent years due to its applications in quantum information processing, quantum sensing and in spintronics [7].

Research in cavity magnonics has been driven by a number of theoretical and experimental efforts. Soykal and Flatté [4] first theoretically predicted a strong interaction of several GHz between magnons and photons in a photonic cavity, and presented the full quantum Hamiltonian of the cavity magnonic system. In their work, they suggested the use of YIG ($Y_3Fe_5O_{12}$) sphere owing to its low dissipation rate, large spin density and high tunability that makes it desirable for coherent information processing [8, 9, 10]. In a subsequent study, Huebl *et al.* carried out a first-of-its-kind experiment that demonstrated the existence of a strong coupling between microwave photons and magnons [11]. The feature depicting the coupling - an anticrossing (or level repulsion) in the eigenspectrum was measured using microwave transmission. That study facilitated the advancement of microwave cavity magnonics.

Since then, there have been a number of theoretical [12, 13] and experimental [14, 15, 16] works on cavity magnon-optical photon coupling leading to the observation of several interesting phenomena, such as the realization of dissipative magnon-photon coupling [17, 18] in which energy transfer between the magnons and photons occurs without maintaining a coherent phase relationship. This coupling can lead to non-Hermitian physics [19, 20] that is significantly different from the effects of coherent magnon-photon coupling [21]. An example of such non-Hermitian physics is level attraction, a phenomenon characterized by complex eigenvalues and the coalescence of energy levels of the interacting system. A number of experiments have also demonstrated the coupling between magnons and optical photons [22, 23, 7, 16] supporting the tuning of magnons using optical field leading to the realization of nonlinear effects in cavity magnonics [12, 24, 25]. Also, the possibility of coupling complex patterns of magnetization to cavity photons has been demonstrated first with a magnetic vortex [26] and later with a ferromagnetic domain wall [27]. In particular, the study in Ref. [27] demonstrated that in an electromagnetic cavity, topological magnetic textures can couple to cavity photons through the inverse Faraday effect. The optomagnonic Hamiltonian in the model can also be used to realize optomagnonic features, most notably, level attraction.

Meanwhile, in recent years, interfacial effects have revealed the possibility of tuning the width

and chirality of domain walls in magnetic materials [28]. One such effect is the Dzyaloshinskii-Moriya interaction (DMI), an antisymmetric exchange interaction in systems with broken inversion symmetry [29]. DMI favors non-parallel alignment of neighboring spins and is known for its role in the formation of structures like skyrmions, which belong to the class of complex patterns of magnetization [30]. Analytical and simulation studies focusing on the effect of DMI in antiferromagnets have shown that this effect can influence both static and dynamical properties of domain walls [29]. For example, it has been shown that the presence of DMI could tilt the easy plane of a domain wall in one configuration, reducing the width of the domain wall, and in another configuration, can play a role in determining the chirality of the domain wall [29]. Many of the studies involving domain walls have been focused on ferromagnets; however, there is significant difference between the dynamics in ferromagnets and antiferromagnets (AFM). For example, unlike ferromagnets, there is no presence of Walker breakdown in AFMs. This is considered an advantage over ferromagnets for certain applications such as fast, energy-efficient data transfer [31, 32, 33]. According to Ref. [31], the non-existence of Walker breakdown can be attributed to the cancellation of the torques that cause tilting in the two sublattices of the antiferromagnet.

In the first part of this thesis, we examine the interaction of photons in a cavity with an antiferromagnetic domain wall. While most cavity magnonic studies have involved ferromagnets, which are characterized by frequencies in the GHz range [34, 23, 35, 11, 15, 22, 16], antiferromagnets can exhibit THz dynamics [36], typically characterized by zero net magnetization and large anisotropies, which are attractive for spintronic applications. Considering that antiferromagnets are potential platforms for exotic spin textures such as skyrmions, which can exist in materials that lack inversion symmetry, we consider the Dzyaloshinskii-Moriya interaction (DMI) in our study. The first project in this thesis attempts to unravel how DMI can affect the coupling of spin textures to optical photons.

A recent experiment proposed a new method for tuning magnon-photon coupling through the use of a low-frequency periodic external field called Floquet drive [37], thereby leveraging time periodicity to investigate the properties of cavity magnonic systems. The experimental set up described in Ref. [37] was used to achieve coherent coupling between magnons and photons within a microwave cavity. The cavity response reveals the realization of level repulsion, an anti-crossing between the magnon and cavity modes. In the second project included in this thesis, we illustrate how level attraction can

be achieved in a periodically-driven system. The techniques used in chapter 3 open up the possibility of studying cavity magnonics semi-classically. This facilitates the investigation of these systems numerically to allow for the study of photon-magnon interaction using micromagnetic simulations. In our study of a magnon-photon system, where the magnetic system is driven out of equilibrium, we realized level attraction. We present a perspective from which level attraction is understood as an instability resulting from the interaction between cavity photons and excitations above a stationary driven magnetization P-mode. We demonstrate that this instability occurs when the cavity resonance is close to the frequency of the lower sideband around the P-mode [38].

Bibliography

[1] J. H. E. Griffiths. Anomalous high-frequency resistance of ferromagnetic metals. *Nature*, 158:670–671, 1946.

[2] L. Landau and E. Lifshitz. On the theory of the dispersion of magnetic permeability in ferromagnetic bodies reprinted from physikalische zeitschrift der sowjetunion 8, part 2, 153, 1935. In L.P. PITAEVSKI, editor, *Perspectives in Theoretical Physics*, pages 51–65. Pergamon, Amsterdam, 1992.

[3] Thomas L. Gilbert. A lagrangian formulation of the gyromagnetic equation of the magnetization field. *Physical Review D*, 100:1243, 1955.

[4] Ö. O. Soykal and M. E. Flatté. Strong field interactions between a nanomagnet and a photonic cavity. *Physical Review Letters*, 104(7), feb 2010.

[5] Jasmin Graf, Hannes Pfeifer, Florian Marquardt, and Silvia Viola Kusminskiy. Cavity optomagnonics with magnetic textures: Coupling a magnetic vortex to light. *Physical Review B*, 98, 12 2018.

[6] Gerrit E. W. Bauer, Eiji Saitoh, and Bart J. van Wees. Spin caloritronics. *Nature Materials*, 11(5):391–399, May 2012.

[7] Dany Lachance-Quirion, Yutaka Tabuchi, Arnaud Gloppe, Koji Usami, and Yasunobu Nakamura. Hybrid quantum systems based on magnonics. *Applied Physics Express*, 12(7):070101, jun 2019.

[8] Xufeng Zhang, Chang-Ling Zou, Liang Jiang, and Hong X. Tang. Cavity magnomechanics. *Science Advances*, 2(3), 2016.

[9] Andrii Chumak, Vitaliy Vasyuchka, Alexander Serga, and Burkard Hillebrands. Magnon spintronics. *Nature Physics*, 11:453–461, 06 2015.

[10] Y Kajiwara, K Harii, Satoru Takahashi, Jannatul Ohe, K Uchida, M Mizuguchi, H Umezawa, H Kawai, K Ando, Kotaro Takanashi, S Maekawa, and E Saitoh. Transmission of electrical signals by spin-wave interconversion in a magnetic insulator. *Nature*, 464:262–6, 03 2010.

[11] Hans Huebl, Christoph W. Zollitsch, Johannes Lotze, Fredrik Hocke, Moritz Greifenstein, Achim Marx, Rudolf Gross, and Sebastian T. B. Goennenwein. High cooperativity in coupled microwave resonator ferrimagnetic insulator hybrids. *Phys. Rev. Lett.*, 111:127003, Sep 2013.

[12] Silvia Viola Kusminskiy, Hong X. Tang, and Florian Marquardt. Coupled spin-light dynamics in cavity optomagnonics. *Phys. Rev. A*, 94:033821, Sep 2016.

[13] Tianyu Liu, Xufeng Zhang, Hong X. Tang, and Michael E. Flatté. Optomagnonics in magnetic solids. *Phys. Rev. B*, 94:060405, Aug 2016.

[14] J. A. Haigh, A. Nunnenkamp, A. J. Ramsay, and A. J. Ferguson. Triple-resonant brillouin light scattering in magneto-optical cavities. *Phys. Rev. Lett.*, 117:133602, Sep 2016.

[15] Xufeng Zhang, Na Zhu, Chang-Ling Zou, and Hong X. Tang. Optomagnonic whispering gallery microresonators. *Phys. Rev. Lett.*, 117:123605, Sep 2016.

[16] A. Osada, R. Hisatomi, A. Noguchi, Y. Tabuchi, R. Yamazaki, K. Usami, M. Sadgrove, R. Yalla, M. Nomura, and Y. Nakamura. Cavity optomagnonics with spin-orbit coupled photons. *Phys. Rev. Lett.*, 116:223601, Jun 2016.

[17] M. Harder, Y. Yang, B. M. Yao, C. H. Yu, J. W. Rao, Y. S. Gui, R. L. Stamps, and C.-M. Hu. Level attraction due to dissipative magnon-photon coupling. *Phys. Rev. Lett.*, 121:137203, Sep 2018.

[18] Biswanath Bhoi, Bosung Kim, Seung-Hun Jang, Junhoe Kim, Jaehak Yang, Young-Jun Cho, and Sang-Koog Kim. Abnormal anticrossing effect in photon-magnon coupling. *Phys. Rev. B*, 99:134426, Apr 2019.

[19] Dengke Zhang, Xiao-Qing Luo, Yi-Pu Wang, Tie-Fu Li, and JQ You. Observation of the exceptional point in cavity magnon-polaritons. *Nature Communications*, 8(1):1368, 2017.

[20] Yunshan Cao and Peng Yan. Exceptional magnetic sensitivity of $\mathcal{PT}$-symmetric cavity magnon polaritons. *Phys. Rev. B*, 99:214415, Jun 2019.

[21] M. Harder, B. M. Yao, Y. S. Gui, and C.-M. Hu. Coherent and dissipative cavity magnonics. *Journal of Applied Physics*, 129(20), 05 2021. 201101.

[22] J. A. Haigh, S. Langenfeld, N. J. Lambert, J. J. Baumberg, A. J. Ramsay, A. Nunnenkamp, and A. J. Ferguson. Magneto-optical coupling in whispering-gallery-mode resonators. *Phys. Rev. A*, 92:063845, Dec 2015.

[23] Yutaka Tabuchi, Seiichiro Ishino, Toyofumi Ishikawa, Rekishu Yamazaki, Koji Usami, and Yasunobu Nakamura. Hybridizing ferromagnetic magnons and microwave photons in the quantum limit. *Phys. Rev. Lett.*, 113:083603, Aug 2014.

[24] YongPan Gao, Cong Cao, Yu-Wen Duan, Xiao-Fei Liu, Ting-Tian Pang, Tie-Jun Wang, and Chuan Wang. Magnons scattering induced photonic chaos in the optomagnonic resonators. *Nanophotonics*, 9, 12 2019.

[25] Wenling Xu, Xiao-Fei Liu, Yang Sun, YongPan Gao, Tie-Jun Wang, and Chuan Wang. Magnon-induced chaos in an optical pt -symmetric resonator. *Physical Review E*, 101, 01 2020.

[26] Jasmin Graf, Hannes Pfeifer, Florian Marquardt, and Silvia Viola Kusminskiy. Cavity optomagnonics with magnetic textures: Coupling a magnetic vortex to light. *Physical Review B*, 98, 12 2018.

[27] Igor Proskurin, Alexander S. Ovchinnikov, Jun-ichiro Kishine, and Robert L. Stamps. Cavity optomechanics of topological spin textures in magnetic insulators. *Phys. Rev. B*, 98:220411, Dec 2018.

[28] M. D. DeJong and K. L. Livesey. Analytic theory for the switch from bloch to néel domain wall in nanowires with perpendicular anisotropy. *Phys. Rev. B*, 92:214420, Dec 2015.

[29] Teo Conzelmann, Severin Selzer, and Ulrich Nowak. Domain walls in antiferromagnets: The effect of dzyaloshinskii–moriya interactions. *Journal of Applied Physics*, 127(22):223908, 2020.

[30] Woo Ham, Abdul-Muizz Pradipto, Kay Yakushiji, Kwangsu Kim, Sonny Rhim, Katsumasa Nakamura, Yoichi Shiota, Sanghoon Kim, and Teruo Ono. Dzyaloshinskii–moriya interaction in noncentrosymmetric superlattices. *npj Computational Materials*, 7, 12 2021.

[31] Severin Selzer, Unai Atxitia, Ulrike Ritzmann, Denise Hinzke, and Ulrich Nowak. Inertia-free thermally driven domain-wall motion in antiferromagnets. *Phys. Rev. Lett.*, 117:107201, Aug 2016.

[32] See-Hun Yang, Kwang-Su Ryu, and Stuart Parkin. Domain-wall velocities of up to 750 m s1 driven by exchange-coupling torque in synthetic antiferromagnets. *Nature nanotechnology*, 10, 02 2015.

[33] Majd Kuteifan, M. V. Lubarda, S. Fu, R. Chang, M. A. Escobar, S. Mangin, E. E. Fullerton, and V. Lomakin. Large exchange-dominated domain wall velocities in antiferromagnetically coupled nanowires. *AIP Advances*, 6(4):045103, 04 2016.

[34] Maxim Goryachev, Warrick G. Farr, Daniel L. Creedon, Yaohui Fan, Mikhail Kostylev, and Michael E. Tobar. High-cooperativity cavity qed with magnons at microwave frequencies. *Phys. Rev. Applied*, 2:054002, Nov 2014.

[35] Xufeng Zhang, Chang-Ling Zou, Liang Jiang, and Hong X. Tang. Strongly coupled magnons and cavity microwave photons. *Phys. Rev. Lett.*, 113:156401, Oct 2014.

[36] V. Baltz, A. Manchon, M. Tsoi, T. Moriyama, T. Ono, and Y. Tserkovnyak. Antiferromagnetic spintronics. *Rev. Mod. Phys.*, 90:015005, Feb 2018.

[37] Jing Xu, Changchun Zhong, Xu Han, Dafei Jin, Liang Jiang, and Xufeng Zhang. Floquet cavity electromagnonics. *Phys. Rev. Lett.*, 125:237201, Dec 2020.

[38] Igor Proskurin, Jephthah O. Iyaro, and Robert L. Stamps. Mode attraction in floquet systems with memory: Application to magnonics. *Phys. Rev. B*, 105:224420, Jun 2022.

Chapter 2

Collective dynamics of an antiferromagnetic domain wall in an optical cavity

Cavity optomagnonics in which precision measurements of interactions between photons and magnons are studied [1] has potential applications in quantum information processing [2] and spintronics [3]. Essentially, it allows a description where the force on magnetic moments appears as an optical pressure of photons. We discuss here an optomagnonic analog of cavity optomechanics [4] in which one is able to observe the coupling of electromagnetic radiation to spin texture oscillations [5, 1]. As a consequence, one is able to realize optomechanical phenomena in magnonic systems, which includes mode attraction - the coalescence of two eigenmodes marked by two exceptional points [6]. Described as an anticrossing gap in Ref. [7] where the coupling between a microwave cavity mode and a ferromagnetic magnon mode was studied, this behaviour has continued to gain attention and has been observed experimentally in the microwave regime in a planar geometry [8] and in a microwave cavity [9] with frequencies in GHz range. The physical mechanisms behind level attraction in these cavity-magnonic experiments have been studied to reveal it is caused by dissipative coupling

[1]DOI: https://doi-org.uml.idm.oclc.org/10.1103/PhysRevB.104.184416

[10, 11, 12] and also attributed to an instability in optomechanical systems associated with a negative frequency in the effective Hamiltonian of an externally driven system [13, 14].

Cavity magnonics has been explored primarily for ferromagnetic systems, with frequencies in the GHz range [15, 16, 17, 18, 19, 20, 21]. At present, antiferromagnets are receiving attention as possible platforms for exotic spin textures such as skyrmions, which can exist in low-dimensional materials with broken inversion symmetry. Antiferromagnets are characterized by dynamics in the THz range [22], typically having large magnetic anisotropies and zero net magnetization that make them useful for spintronic applications, but at the same time makes experimental observation of collective magnetic dynamics difficult. Here, we propose to use magneto-optical coupling, which is a well established experimental technique to study ultrafast dynamics in antiferromagnetic insulators [23] to study the collective motion of antiferromagnetic textures.

The Dzyaloshinskii-Moriya interaction (DMI) can exist in non-centrosymmetric magnetic materials and is known to play an important role in describing non-trivial spin textures [24, 25]. In one spatial dimension, DMI can lead to long-periodic modulated structures known as soliton lattices, while in two spatial dimensions DMI helps to stabilize topologically non-trivial skyrmion lattices. It is also known to play an important role in domain walls [26, 27], where it affects the domain wall structure and lifts degeneracy between domain walls with opposite chiralities. In this paper, we show that DMI can also affect how spin textures are coupled to optical photons.

Optomagnonics opens the possibility of coupling electromagnetic waves to non-uniform magnetic ground states such as a magnetic vortex in a microdisk [28]. Whereas some of the most interesting textures are found in two and three dimensions, there have been some studies on one-dimensional structures such as solitons in antiferromagnets [29, 30, 31] and helimagnets [32, 33]. Here, we examine the case of the coupling of optical cavity photons to a domain wall. Domain walls are one-dimensional topological textures whose dynamics can be described in analogy to that of massive particles [34, 35]. The collective motion of ferromagnetic and antiferromagnetic domains walls is well studied [36, 37, 38, 35, 39, 40, 41].

Coupling of collective magnon modes to optical cavity modes have been realized in a number of experiments [20, 42]. Recently, a model for cavity magnonics with a ferromagnetic domain wall was proposed and parameters for the coupling were estimated [43]. In that case the frequency of the

ferromagnetic domain wall oscillation in a pinning site is in the GHz range.

In this paper, we discuss a cavity optomagnonic system where an antiferromagnetic domain wall is coupled to optical photons via the inverse Faraday effect [44, 45, 23]. This leads to a non-linear optomechanical-type coupling where the domain wall reacts to pressure from cavity photons. We discuss the hybridization of optical and magnonic modes, and identify a level attraction regime.

We also investigate the effects of DMI on the domain wall dynamics in two different geometries. We find that in one geometry, where DMI favours one chirality of the domain wall, the presence of DMI enables coupling of magnons to photons which is otherwise non-existent without DMI. In a second geometry, the DMI exerts a torque which leads to the domain wall tilt and consequent effects on the coupling terms. We expect that these features are not limited to the case of a single domain wall and can be found in other chiral spin textures. This can assist detection and quantification of DMI in thin films of antiferromagnetic materials.

2.1 The model

Our model assumes a Néel domain wall in a one-dimensional antiferromagnet as shown in Fig. (2.1 a). Sublattices A and B have opposite spins, S_{A} and S_{B}, respectively. The preferred magnetization rotation plane is the x-z plane. The Hamiltonian describing this system is:

$$\mathcal{H}_{\mathrm{dw}} = \sum_{\langle i,j \rangle} J\vec{S}_i \cdot \vec{S}_j - K_z \sum_i (\vec{S}_{i,z})^2 - \sum_i K_x (\vec{S}_{i,x})^2 + \sum_i (-1)^{i+1} \vec{D} \cdot (\vec{S}_i \times \vec{S}_{i+1}). \tag{2.1}$$

The first term on the right is the nearest-neighbour exchange interaction between spins on the sublattices. The second and third terms are the uniaxial anisotropies in the z and x directions, respectively [46] with constants $K_z \gg K_x$. The last term is the antisymmetric interfacial DMI whose alternating sign prevents a spiral spin state [47].

We introduce the total and staggered magnetizations, $\vec{m}_i = (\vec{S}^i_A + \vec{S}^i_B)/2S$ and $\vec{l}_i = (\vec{S}^i_A - \vec{S}^i_B)/2S$, respectively, subject to the constraints that $\vec{m} \cdot \vec{l} = 0$ and $\vec{m}^2 + \vec{l}^2 = 1$ [48, 38, 35, 49]. Going by this definition, we make the substitutions, $\vec{S}^i_A = S(\vec{m}_i + \vec{l}_i)$ and $\vec{S}^i_B = S(\vec{m}_i - \vec{l}_i)$ into Eq. (2.1). This results in a sum over lattice points rather than spins. We simplify the non-DMI part of the Hamiltonian

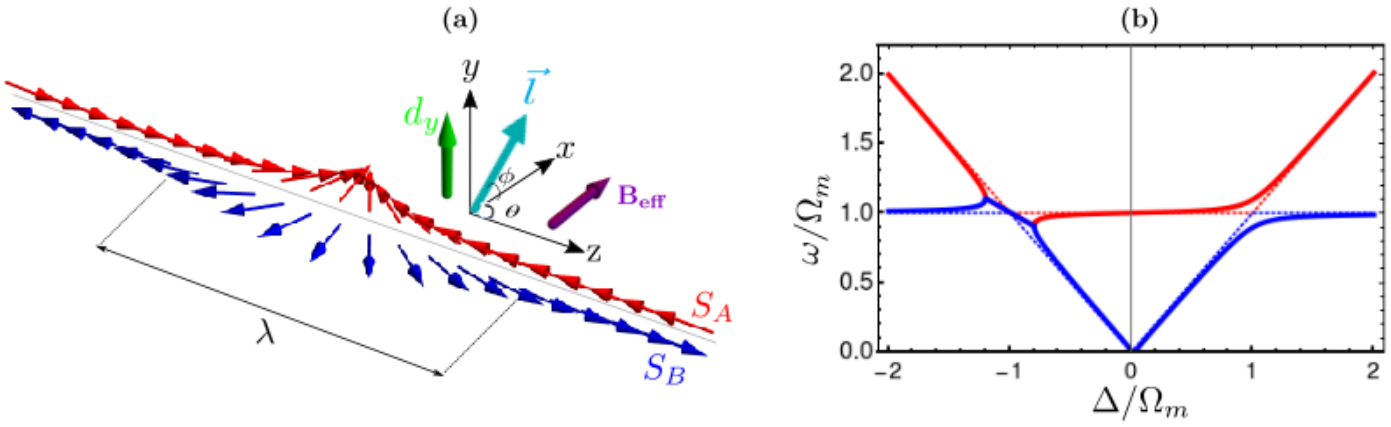

Figure 2.1: (a) Schematic illustration of the geometry where the effective magnetic field of the light along $\hat{x}$ interacts with the domain wall with width λ and axis along $\hat{z}$ in the presence of DMI along $\hat{y}$. (b) Hybridized frequency of the cavity modes and magnon modes of the antiferromagnetic domain wall as a function of the detuning parameter in the absence of DMI. In the absence of DMI, there is no coupling achieved as indicated by the dotted lines. The thick lines represent what happens in the presence of DMI when the magnon modes couple to the cavity modes. The real part of the two modes attract in the region of negative detuning and repulsion is observed in the region of positive detuning.

based on the approach in Ref. [38] by introducing the following identities: $2\vec{m}_i\vec{m}_{i+1} = \vec{m}_i^2 + \vec{m}_{i+1} - (\vec{m}_{i+1} - \vec{m}_i)^2$ and $(\vec{l}_i\vec{m}_{i+1} - \vec{m}_i\vec{l}_{i+1}) = \vec{l}_i(\vec{m}_{i+1} - \vec{m}_i) - \vec{m}_i(\vec{l}_{i+1} - \vec{l}_i)$. The simplification of the DMI term is included in Appendix B. It is useful make a continuum approximation, $\vec{m}_{i+1} \approx \vec{m}_i + a_0(\partial\vec{m}_i/\partial z) + ...$ and $\vec{l}_{i+1} \approx \vec{l}_i + a_0(\partial\vec{l}_i/\partial z) + ...$, where a_0 is the lattice constant. In Eq. (2.1), we replace $\vec{m}_i$ and $\vec{l}_i$ by $\vec{m}(z)$ and $\vec{l}(z)$, respectively, and the sums are replaced by integrals. We describe the dynamics of the AFM in the exchange approximation and consider a slowly varying AFM domain wall. In this description, the exchange interaction is much larger than the anisotropic terms and $|\vec{m}|^2 \ll |\vec{l}|^2$. Thus, the anisotropic terms proportional to the total magnetization can be neglected [38, 50] (details are provided in Appendix A). Adding the DMI term, our expression in the continuum model is similar to that in Ref. [24]:

$$\mathcal{H}_{\rm dw} = \int_{-\infty}^{\infty} \frac{dz}{a_0}\left[\frac{a}{2}|\vec{m}|^2 + \frac{A}{2}\left|\frac{\partial\vec{l}}{\partial z}\right|^2 + L\left(\vec{m}\cdot\frac{\partial\vec{l}}{\partial z}\right) - \frac{k_z}{2}(\vec{l}\cdot\hat{z})^2 - \frac{k_x}{2}(\vec{l}\cdot\hat{x})^2 + \vec{d}\cdot(\frac{\partial\vec{l}}{\partial z}\times\vec{l}) + \vec{d}_0\cdot(\vec{m}\times\vec{l})\right], \tag{2.2}$$

where $a = 8JS^2$ and $A = a_0^2JS^2$ are the homogenous and non-homogenous exchange constants, respectively, $L = 2a_0JS^2$ is the parity-breaking term [38, 24], the anisotropies are $k_z = 2K_zS^2$ and $k_x = 2K_xS^2$, and the DMI coefficients are $\vec{d} = a_0S^2\vec{D}$ and $\vec{d}_0 = 4S^2\vec{D}$.

The Lagrangian of the system, $\mathcal{L} = \mathcal{L}_B - \mathcal{H}_{\rm dw}$ is constructed using the Berry phase, $\mathcal{L}_B =$

$2\hbar S\ \vec{m}(\partial_t \vec{l} \times \vec{l})$ [38, 40, 24], which accounts for the inertia of the antiferromagnetic domain wall. By varying the Lagrangian with respect to $\vec{m}$, we derive an expression for $\vec{m}$ in terms of the temporal and spatial derivative of $\vec{l}$:

$$\vec{m} = \frac{\rho}{a}\left(\vec{l} \times \frac{\partial \vec{l}}{\partial t}\right) - \frac{L}{a}\left(\frac{\partial \vec{l}}{\partial z}\right) + \frac{1}{a}\vec{d}_0 \times \vec{l}, \tag{2.3}$$

where $\rho = 2\hbar S$. Eq. (2.3) which implies that $\vec{m}$ is a slave variable to $\vec{l}$ [38, 24] is substituted into Eq. (2.2), making it possible to eliminate $\vec{m}$ from Eq. (2.2)). We simplify Eq. (2.2) and disregard the total time derivatives proportional to the homogenous DMI and terms proportional to the topological term, L that do not contribute to the equations of motion [24] (see Appendix A for details). The Hamiltonian is thus:

$$\mathcal{H}_{\rm dw} = \int_{-\infty}^{\infty} \frac{dz}{a_0}\left[\frac{\rho^2}{2a}\left(\frac{\partial \vec{l}}{\partial t}\right)^2 + \frac{A}{2}\left|\frac{\partial \vec{l}}{\partial z}\right|^2 - \frac{k_z}{2}(\vec{l}\cdot\hat{z})^2 - \frac{k_x}{2}(\vec{l}\cdot\hat{x})^2 + \vec{d}\cdot\left(\frac{\partial \vec{l}}{\partial z} \times \vec{l}\right)\right], \tag{2.4}$$

We parameterize the staggered magnetization, $\vec{l}$ by polar and azimuthal angles θ and ϕ in spherical coordinates: $\vec{l} = (\sin\theta\cos\phi, \sin\theta\sin\phi, \cos\theta)$. For the static wall configuration, $\partial\vec{l}/\partial t = 0$ in Eq. (2.4). By this definition, the Hamiltonian of the system is:

$$\mathcal{H}_{\rm dw} = \int_{-\infty}^{\infty} \frac{dz}{a_0}\left[A\left(\frac{\partial\theta}{\partial z}\right)^2 - k_x \sin^2\theta\cos^2\phi - k_z\cos^2\theta - d_x\left(\frac{\partial\theta}{\partial z}\right)\sin\phi + d_y\left(\frac{\partial\theta}{\partial z}\right)\cos\phi\right], \tag{2.5}$$

where d_x and d_y are the x and y components of the DMI, respectively. The domain wall static profile is obtained using the standard methods [46, 51, 52, 38, 49]. The domain wall tilt angle is defined as ϕ with respect to the x-z plane and assumed to be constant throughout the wall [46]. The energy density is minimized via the Euler-Lagrange equation giving a wall profile $\theta(z) = 2\tan^{-1}\exp((z - z_0)/\lambda)$, where $\lambda = \sqrt{A/(k_z - k_x\cos^2\phi)}$ is the characteristic domain wall width. Our analysis of the static wall profile dependence on DMI agrees with the results in Ref. [46]. We summarize the key details in subsequent paragraphs.

The wall energy, $\mathcal{E} = 4\sqrt{A(k_z - k_x\cos^2\phi)} - d_x\pi\sin\phi + d_y\pi\cos\phi$ is obtained by substituting the wall profile into Eq. (2.5) and integrating with respect to z. Since the energy density depends on only

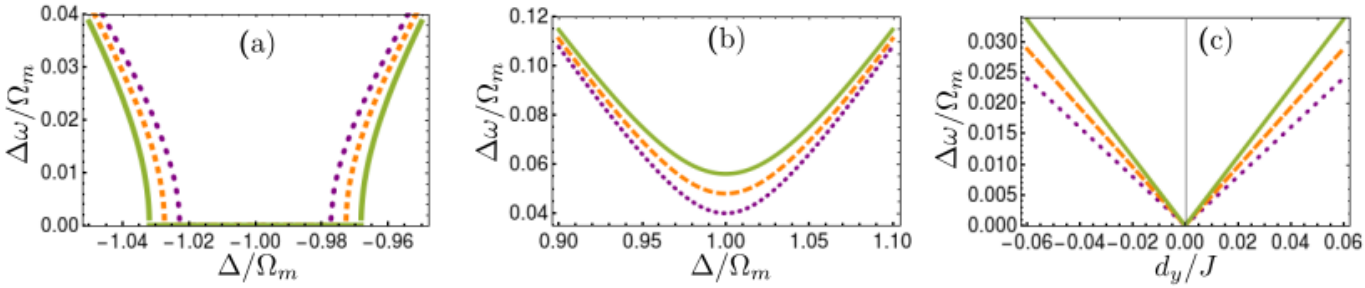

Figure 2.2: (a) Frequency gap in the presence of DMI of strength $0.06J$ as a function of the negative detuning around the point of attraction for different coupling strengths: $g = 0.10$ MHz, $g = 0.12$ MHz, and $g = 0.14$ MHz represented by the purple dotted, orange dashed and green solid lines, respectively. Around the exceptional point, attraction dominates a wider range for larger coupling strengths and decreases for lower coupling strengths. (b) Frequency gap in the presence of DMI of strength $0.06J$ as a function of the positive detuning. For the same value of detuning, larger frequency gaps are observed for larger coupling. In all cases, the gap is minimum at resonance and increases as we move away from resonance. (c) Frequency gap as a function of negative and positive DMI present along the $\hat{y}$. At $d_y = 0$ there is no gap. In the presence of DMI, the frequency gaps increase linearly with increasing magnitude of DMI and the gap is observed to be larger for larger coupling strengths.

the x and y components of the DMI, two DMI directions are considered. When coupling the domain wall to the cavity modes, we find that the direction of photon propagation must be perpendicular to both the DMI and the domain wall axis (z axis) in order for coupling to be achieved. This requires two possible geometries to be considered.

First, DMI is considered to be present in the $\hat{x}$ direction. This results in a distortion of the spin orientation on the sublattices and consequently results in a DMI-dependent tilt angle [46],

$$\phi(d_x) = \text{sgn } d_x \cdot \cos^{-1}\left(\pm\sqrt{\frac{(8Jk_x^2 - d_x^2 k_z \pi^2)}{(8Jk_x^2 - d_x^2 k_x \pi^2)}}\right), \tag{2.6}$$

which minimizes the energy density. This dependence remains valid until a saturated DMI strength of $d_{x,\text{sat}} = 4/\pi\sqrt{Jk_x^2/2k_z}$ is reached beyond which $\phi(d_x) = \pi/2$.

For the second geometry where DMI is present along $\hat{y}$, the DMI rather breaks the degeneracy of the domain wall energy minima and favours one chirality of the wall at a critical value, $d_{y,\text{c}} = 4k_x/\pi\sqrt{J/2(k_z - k_x)}$. The tilt angle, $\phi(d_y) = 0$ if $d_y < d_{y,\text{c}}$. Otherwise, $\phi(d_y) = \pi$ [46].

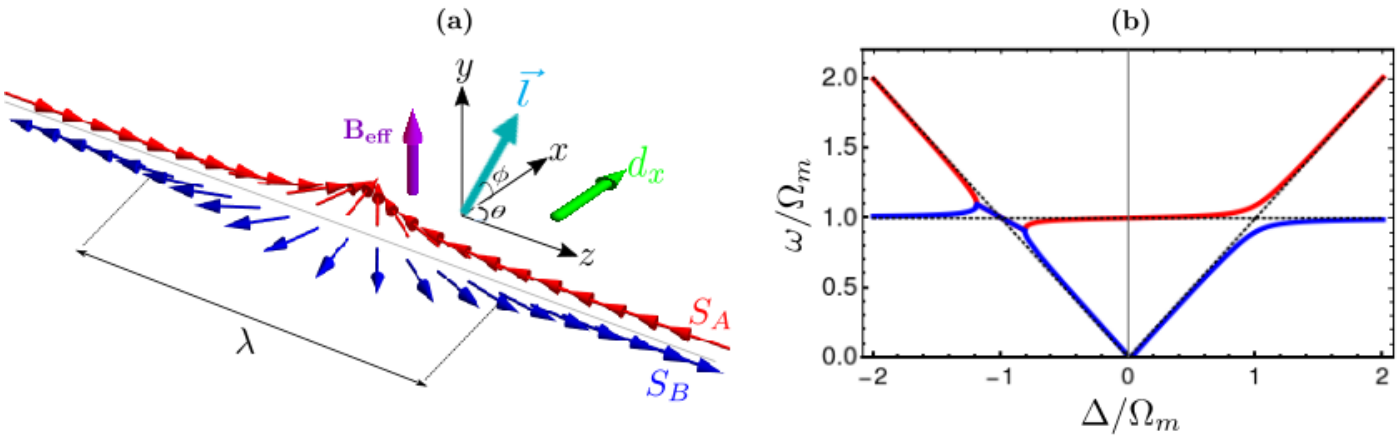

Figure 2.3: (a) Schematic illustrating the geometry where the effective magnetic field of the light along $\hat{y}$ interacts with the domain wall of width, λ with axis along $\hat{z}$ in the presence of DMI along $\hat{x}$. (b) Hybridized frequency of the cavity modes and magnon modes of the antiferromagnetic domain wall as a function of the detuning parameter in the absence of DMI. The red and blue thick lines indicate coupling between the magnonic and photonic modes in the absence of DMI. The real part of the two modes attract in the region of negative detuning and repulsion is observed in the region of positive detuning. As the magnitude of DMI increases, coupling between modes reduces until no coupling is achieved. The black dotted lines show that there is no coupling at the saturated value of DMI.

2.2 Domain wall dynamics

We discuss the effects of DMI on the dynamics of an antiferromagnetic domain wall when coupled to optical photons in an electromagnetic cavity. The dynamics of the antiferromagnet is described in the semi-classical approximation. For this purpose, the Lagrangian of the system, $\mathcal{L} = \mathcal{L}_B - \mathcal{H}_{\rm dw}$ [24], where the first term corresponds to the Berry phase [38, 40, 24] and the second term is the magnetic energy in Eq. (2.5). We describe the domain wall dynamics using the collective coordinate method [35, 53], treating the position of the domain wall $Z_0(t)$ as a dynamical variable.

The effective Lagrangian in terms of the domain wall position $Z_0(t)$ and small fluctuations around the domain wall profile, $\delta\theta(t)$, is obtained from Eq. (2.5) by performing the expansion, $\phi(z,t) = \phi_0(z - Z_0(t))$ and $\theta(z,t) = \theta_0(z - Z_0(t)) + \delta\theta(z - Z_0(t))$. For the fluctuations $\delta\theta(t)$, we obtain the Pöschl-Teller equation. The solution is $\delta\theta = p(t)\ \mathrm{sech}[(z - Z_0(t))/\lambda]$, where p is the amplitude of the out-of-plane component.

In order to fully describe the dynamics of the antiferromagnetic domain wall, we include a pinning potential. The pinning potential provides a restoring force and is introduced as a point defect which contributes to the anisotropy along $\hat{y}$ at $z = 0$. The pinning potential, $V_{pin} = -K_{pin} \int [\frac{dz}{a_0} \delta(z) \sin^2\theta(z) \sin^2\phi(z)] \approx K_{pin}\ Z_0^2/\lambda^2$. We proceed to construct the total Lagrangian of

the system following the approach in Ref. [24]. The effective Lagrangian for the collective coordinate $Z_0(t)$ in addition to the pinning potential, $\mathcal{L} = \mathcal{L}_B - \mathcal{H}_{\rm dw} - V_{\rm pin}$ is expressed below:

$$\mathcal{L} = \frac{1}{a_0}\left(\frac{2\rho^2}{a\lambda}\dot{Z}_0^2 - \frac{a_0 K_{\rm pin}}{\lambda^2}Z_0^2 - 2A\lambda + 2K_x\cos^2\phi - \pi\lambda d_x\sin\phi + \pi\lambda d_y\cos\phi\right). \tag{2.7}$$

We define the generalized momentum, $P_z = \partial\mathcal{L}/\partial\dot{Z}_0 = (4\rho^2/a_0\lambda)$ and $\dot{Z}_0 = (a_0\lambda P_z)/(4\rho^2)$.

From the Lagrangian in Eq. (2.7), we transform to the Hamiltonian description. The Hamiltonian of the pinned domain wall, excluding terms that do not contribute to the equations of motion can then be written in terms of the wall position as:

$$\mathcal{H}'_{\rm dw} = \frac{2\rho^2\dot{Z}_0^{\,2}}{a_0\ a\lambda} + \frac{K_{\rm pin}Z_0^2}{2} \tag{2.8}$$

where we have dropped terms proportional to the out-of-plane component.

The Hamiltonian in Eq. (2.8) shows that the low energy motion of the pinned domain wall is similar to that of a massive particle in a parabolic potential. This motion can be quantized using a standard quantum-mechanical method of the quantization of a harmonic oscillator. From Eq. (2.8), we derive the canonical conjugate momentum P_{Z_0} corresponding to Z_0, and the Hamiltonian is quantized by making the transformations: $\hat{Z}_0 = \sqrt{\hbar/2M\Omega_m}(\hat{b}+\hat{b}^\dagger)$ and $\hat{P}_{Z_0} = -i\sqrt{\hbar M\Omega_m/2}(\hat{b}-\hat{b}^\dagger)$, where $\hat{b}$ and $\hat{b}^\dagger$ are the annihilation and the creation operators of the oscillator in Eq. (2.8), M is the domain wall effective mass and Ω_m is the characteristic oscillation frequency of the domain wall.

The coupling mechanism between the domain wall and cavity photon is assumed to be the inverse Faraday effect [44]. In this way, the coupling appears as a reaction force to photon pressure exerted as compensation to changes in photon polarisation. Details can be found in Ref. [43, 54, 55, 23, 56]. The magneto-optical interaction energy [56] is expressed as:

$$\mathcal{H}_{\rm mo} = -\frac{i}{4}f\epsilon_0\int d^3r\ \vec{m}(\vec{r})\cdot[\vec{E}^*(\vec{r},t)\times\vec{E}(\vec{r},t)], \tag{2.9}$$

where $\vec{m}$ is the total magnetization vector, f is the Faraday rotation material-dependent parameter, ϵ_0 is the permittivity of free space and $\vec{E}$ is the electric field vector of light. In this work, $\vec{m}$ is given by Eq. (2.3).

The first of the two geometries considered is that in which there is electromagnetic wave propagating along $\hat{x}$, and circularly polarized in y-z plane. In this geometry, the resulting effective magnetic field of light in Eq. (2.9) is given by $\vec{E}^*(x) \times \vec{E}(x) = \hat{x}\ (i\hbar\omega)/(2V\epsilon_0)[\hat{a}_R^\dagger \hat{a}_R - \hat{a}_L^\dagger \hat{a}_L]$, where V is the volume of the cavity and $\hat{a}_{R(L)}$ is related to the right (left) circularly polarized basis. The magneto-optical Hamiltonian obtained from Eq. (2.9), considering only the right-circular polarization is $\mathcal{H}^x_{\rm mo}$ $= (-if/4)(A_\perp/2V)[(-\rho/a)\sin\phi \dot{Z}_0 + (2d_y/a)Z_0]\hbar\omega_c \hat{a}_R^\dagger \hat{a}_R$, where $A_\perp$ is the sample cross section. This shows that the interaction along $\hat{x}$ is proportional to the tilt angle of the domain wall and the y component of the DMI (perpendicular to both the wall axis and the direction of propagation of electromagnetic waves).

In addition, we introduce the photonic Hamiltonian, $\mathcal{H}_{\rm ph} = \hbar\omega_c \hat{a}^\dagger \hat{a}$ and an external laser driving term, $\mathcal{H}_{\rm drive} = \varepsilon \hat{a}^\dagger e^{-i\omega_d t} + \varepsilon^* \hat{a} e^{i\omega_d t}$, where ε is the pump amplitude and ω_d is the driving frequency. In order to remove the time dependence of the driving terms, we move to a rotating frame defined by the cavity field photon number, rotating at a drive frequency ω_d by performing the unitary transformation $\mathcal{H}'_{\rm (ph,drive)} = -i\hbar(d\hat{U}^\dagger/dt)\hat{U} + \hat{U}\ (\mathcal{H}_{\rm drive} + \mathcal{H}_{\rm ph})\ U^\dagger$, where $\hat{U}(t) = e^{i\hbar\omega_d t \hat{a}^\dagger \hat{a}}$ [4]. This gives $\mathcal{H}'_{\rm (ph,drive)} = -\hbar\Delta \hat{a}^\dagger \hat{a} + \varepsilon \hat{a}^\dagger + \varepsilon^* \hat{a}$, where $\Delta = \omega_d - \omega_c$ is the laser detuning parameter. The effective Hamiltonian of the system is:

$$\mathcal{H}_{\rm tot} = \hbar\Omega_m \hat{b}^\dagger \hat{b} - \hbar\Delta \hat{a}^\dagger \hat{a} + \varepsilon \hat{a}^\dagger + \varepsilon^* \hat{a} - \hbar\ g_0 \left(-i \sin\phi \frac{\hbar\Omega_m}{K_z}(\hat{b} - \hat{b}^\dagger) + \frac{2d_y}{a}(\hat{b} + \hat{b}^\dagger) \right) \hbar\omega_c \hat{a}_{\rm R}^\dagger \hat{a}_{\rm R}, \quad (2.10)$$

where $g_0 = \frac{1}{4} f S_{\rm eff} \omega_c$. $S_{\rm eff} = A_\perp x_{\rm zpf}/V$, where $A_\perp$ is the sample cross section, V is the volume of the cavity, $x_{\rm zpf} = \sqrt{\hbar/(2M\Omega_m)}$. $f = 2c\theta_f\sqrt{\epsilon}/\omega_c$ is the Faraday rotation per length, c is the speed of light in vacuum and ϵ is the dieletric constant of the material. The antiferromagnetic domain wall effective mass is $M = 4\hbar^2/(a_0 K_z \lambda)$ and the characteristic oscillation frequency, $\Omega_m = \sqrt{K_{\rm pin}/(M\lambda^2)}$.

As an example, we estimate values for a common antiferromagnet using experimental data for NiO having a domain wall width of approximately 150 nm [23], $a_0 = 0.418$ nm [57] and $K_z = 4$ K$/k_B$ [58], where k_B is the Boltzmann constant. We assume $K_{\rm pin} = 1$K$/k_B$ such that it is of the same order of magnitude as the anisotropy constant. This gives $M \approx 10^{-29} kg$ and $\Omega_m \approx$ 10 GHz. Due to lack of experimental data on optomagnonic coupling with AFMs, we assume a material size similar to a YIG sphere of diameter 0.25 mm in a cavity having a dimension of $40 \times 25 \times 15$ mm^3 [17] such that

$S_{\text{eff}} \approx 10^{-10}$, $\epsilon = 5$ and $\theta_f = 419$ radm^{-1} [1, 59]. We estimate the coupling strength in Eq. (2.10), $g_0 = c\theta_f\sqrt{\epsilon}S_{\text{eff}}/2 \approx 40.7$ Hz.

The equations of motion for $\hat{a}$, $\hat{a}^\dagger$, $\hat{b}$ and $\hat{b}^\dagger$ in the Appendix are obtained from Eq. (2.10) and linearized by splitting the operators into an average plus a fluctuating term. e.g. $\hat{a} = \langle\hat{a}\rangle + \delta\hat{a}$, where $\langle\hat{a}\rangle$ is related to the average number of cavity photons, $\bar{n}_c = |\langle\hat{a}\rangle|^2$ [4]. Solving the equations of motion for the hybridized frequency ω, we obtain two pairs of eigenmodes:

$$\omega_\pm = \sqrt{\frac{\Delta^2 + \Omega_m^2}{2} \pm \sqrt{\frac{(\Delta^2 - \Omega_m^2)^2}{4} - 16g^2\tilde{d}_y^2\Delta\Omega_m}}, \tag{2.11}$$

where $\tilde{d}_y = d_y/a$ and $g = \sqrt{\bar{n}_c}g_0$ is the measure of the photon-enhanced coupling of magnons to photonic modes. $g \approx 0.1 - 1$ MHz for a microcavity that can support up to $10^7 - 10^9$ photons [1]. Equation (2.11) shows that if there were no coupling (i.e $g = 0$), there would be crossing of the modes. The same result is realized in the absence of DMI since $d_y = 0$ and $\phi(d_y) = 0$ do not provide coupling in Eq. (2.11) . The dotted lines in Fig (2.1 b) show crossing of modes in both regions ($\Delta > 0$ and $\Delta < 0$) when DMI is absent, and no coupling is evident. The thick lines show that in the presence of DMI, degeneracy is broken and avoided crossing of modes is realized for positive detuning ($\Delta > 0$), indicating coherent coupling of the modes. In the region of negative detuning ($\Delta < 0$), there are exceptional points where the eigenfrequencies become complex and there is coalescence of their real parts resulting in mode attraction. In order to illustrate the consequence of the presence of DMI on resonances, we study the frequency gaps, $\Delta\omega = \omega_+ - \omega_-$. In Fig. (2.2), $\Delta\omega$ is shown as a function of Δ for different values of g. In the region of negative detuning (Fig 2.2 a), around the exceptional points, there is no frequency gap and the attraction regime spans a wider range of detuning for increasing coupling strengths. Away from the exceptional points we observe a difference in frequencies of the two modes. On the other hand, in the region of repulsion (Fig. 2.2 b), there exists a frequency gap. This gap can be seen to increase with increasing coupling strength. Fig. (2.2 c) provides a description of how frequency gaps for positive and negative Δ depend on DMI at resonance. The gaps increase with increasing magnitude of DMI and vanish in the absence of DMI. We conclude that the coupling of the photonic mode to the magnonic mode is dependent on the DMI strength.

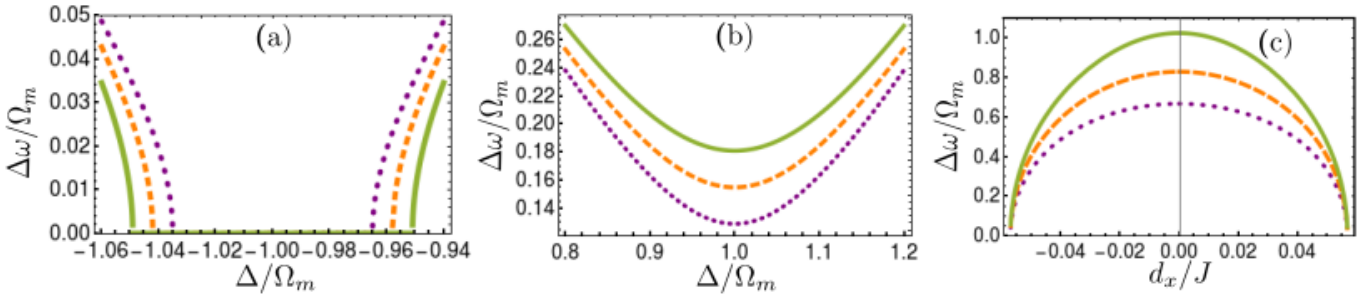

Figure 2.4: The effect of DMI of strength $0.06J$ on the frequency gaps as (a) a function of the negative detuning around the point of attraction for different coupling strengths: $g = 0.10$ MHz, $g = 0.12$ MHz, and $g = 0.14$ MHz represented by the purple dotted, orange dashed and green solid lines, respectively. Around the exceptional point, attraction dominates a wider range for larger coupling strengths and decreases for lower coupling strengths. (b) Frequency gap in the presence of DMI of strength $0.06J$ as a function of the positive detuning. For the same value of detuning, larger frequency gaps are observed for larger coupling. In all cases, the gap is minimum at resonance and increases as we move away from resonance. (c) Frequency gap as a function of negative and positive DMI present along the $\hat{y}$. The values of the coupling strength g become more important as d_x approaches zero. The frequency gap reduces for increasing magnitude of the DMI and vanishes as the saturated value of DMI is reached.

The second geometry considered in this work is the case where the domain wall interacts with waves propagating along $\hat{y}$, and circularly polarized in the x-z plane (Fig 2.3 a). In this geometry, the coupling of cavity modes to the domain wall excitations is realized even in the absence of DMI. We observe that this coupling is stronger than in the first geometry considered due to the fact that the electromagnetic wave is applied in a direction perpendicular to the easy plane of the domain wall, thus maximizing coupling to the variation of magnetization. Following a similar approach described for the first geometry considered, we obtain two pairs of eigenmodes:

$$\omega_{\pm} = \sqrt{\frac{\Delta^2 + \Omega_m^2}{2} \pm \sqrt{\frac{(\Delta^2 - \Omega_m^2)^2}{4} - 16g^2\tilde{d}_x^2\Delta\Omega_m - 2g^2\pi^2\Delta\Omega(1+\cos 2\phi)}}, \tag{2.12}$$

where $\tilde{d}_x = d/a$. Fig. (2.3 b) shows a plot of the hybridized frequency in Eq. (2.12) as a function of the detuning parameter, Δ.

We discuss what happens when DMI is absent ($d_x = 0$). The thick red and blue lines in Fig. (2.3 b) indicate that there is coupling even in the absence of DMI. However, when DMI is present along $\hat{x}$, the spin orientations are distorted out of the plane of the wall and we have a non-zero tilt angle which depends on the DMI strength. This modifies the domain wall width as $\lambda_{d_x} = \sqrt{A/(k_z - k_x(8Jk_x^2 - d_x^2k_z\pi^2)/(8Jk_x^2 - d_x^2k_x\pi^2))}$. The consequence of this is a weaker magneto-

optical coupling in the interaction for both positive and negative values of DMI, and symmetric about $d_x = 0$ up to the saturated value, $d_{\text{sat}} = 4/\pi\sqrt{Jk_x^2/2k_z}$ (when crossing of the modes emerges in both regions). As indicated by the black dotted lines in Fig.(2.3 b), DMI reduces the coupling strength between the modes until crossing of the mode is achieved just as $d_x = d_{\text{sat}}$.

The dependence of the frequency gaps on the detuning in the presence of DMI along x is similar to what we observed along y except that the attraction and repulsion are stronger for the same value of DMI if we compare Figs. (2.2 a) and (2.2 b) to Fig. (2.4 a) and (2.4 b). The most striking feature that distinguishes both geometries is how the frequencies change with respect to the DMI. Contrary to the previous geometry, increase in the DMI applied along x leads to decrease in the frequencies until the gap vanishes at the saturated value of DMI (Fig. 2.4 c). It is useful to define the frequency gap $\Delta\omega(\tilde{d}_x)$ in order to see clearly how the frequency gap depends on DMI at resonance. We calculate this from Eq. (2.12): $\Delta\omega(d_x) = \omega_+ - \omega_-|_{\Omega_m=\Delta=1} \approx 2g(8\tilde{d}_x^2 + \pi^2(1 + \cos 2\phi(\tilde{d}_x)))$. For example, if we assume a coupling strength of 0.1 MHz at a tilt angle of $\pi/2$, then $\Delta\omega \approx 2\tilde{d}_x^2$ MHz. This shows that the gap depends on the DMI constant and may be used to determine the DMI strength for given values of the coupling strength.

2.3 Conclusion

We demonstrated that the collective excitation of a Neél antiferromagnetic domain wall can be realized through magneto-optical coupling to cavity photons. The resulting Hamiltonian is of an optomagnonic type, which allows realization of optomechanical instabilities such as level attraction in a driven system. We find that the presence of DMI enables coupling between a domain wall and cavity photons in a geometry where there is no coupling otherwise. This opens a possibility for estimating DMI in antiferromagnetic materials by measuring the interaction of antiferromagnetic resonances to optical modes in an optical cavity. This approach is not limited to a single domain wall dynamics but applicable to other one dimensional textures like chiral soliton lattice in ferromagnets and antiferromagnets and can, in principle, be extended to antiferromagnetic spin textures in two spatial dimensions such as skyrmions and skyrmion lattices, which remains a future problem.

Bibliography

[1] Silvia Viola Kusminskiy, Hong X. Tang, and Florian Marquardt. Coupled spin-light dynamics in cavity optomagnonics. *Phys. Rev. A*, 94:033821, Sep 2016.

[2] R. Hisatomi, A. Osada, Y. Tabuchi, T. Ishikawa, A. Noguchi, R. Yamazaki, K. Usami, and Y. Nakamura. Bidirectional conversion between microwave and light via ferromagnetic magnons. *Phys. Rev. B*, 93:174427, May 2016.

[3] Alexy D. Karenowska, A. V. Chumak, A. A. Serga, and Burkard Hillebrands. *Magnon Spintronics*, pages 1–38. Springer Netherlands, Dordrecht, 2014.

[4] Markus Aspelmeyer. Cavity optomechanics. *Rev. Mod. Phys*, 86(December), 2014.

[5] N. Brahms and D. M. Stamper-Kurn. Spin optodynamics analog of cavity optomechanics. *Phys. Rev. A*, 82:041804, Oct 2010.

[6] W D Heiss. Exceptional points of non-hermitian operators. *Journal of Physics A: Mathematical and General*, 37(6):2455–2464, jan 2004.

[7] Vahram L. Grigoryan and Ke Xia. Cavity-mediated dissipative spin-spin coupling. *Physical Review B*, 100(1), jul 2019.

[8] Biswanath Bhoi, Bosung Kim, Seung-Hun Jang, Junhoe Kim, Jaehak Yang, Young-Jun Cho, and Sang-Koog Kim. Abnormal anticrossing effect in photon-magnon coupling. *Phys. Rev. B*, 99:134426, Apr 2019.

[9] M. Harder, Y. Yang, B. M. Yao, C. H. Yu, J. W. Rao, Y. S. Gui, R. L. Stamps, and C.-M. Hu. Level attraction due to dissipative magnon-photon coupling. *Phys. Rev. Lett.*, 121:137203, Sep 2018.

[10] Weichao Yu, Jiongjie Wang, H. Y. Yuan, and Jiang Xiao. Prediction of attractive level crossing via a dissipative mode. *Phys. Rev. Lett.*, 123:227201, Nov 2019.

[11] Peng-Chao Xu, J. W. Rao, Y. S. Gui, Xiaofeng Jin, and C.-M. Hu. Cavity-mediated dissipative coupling of distant magnetic moments: Theory and experiment. *Phys. Rev. B*, 100:094415, Sep 2019.

[12] Yi-Pu Wang and Can-Ming Hu. Dissipative couplings in cavity magnonics. *Journal of Applied Physics*, 127(13):130901, 2020.

[13] Igor Proskurin, Rair Macedo, and Robert L. Stamps. Microscopic origin of level attraction for a coupled magnon-photon system in a microwave cavity. *New Journal of Physics*, 21(9), 9 2019.

[14] N. R. Bernier, L. D. Tóth, A. K. Feofanov, and T. J. Kippenberg. Level attraction in a microwave optomechanical circuit. *Phys. Rev. A*, 98:023841, Aug 2018.

[15] Maxim Goryachev, Warrick G. Farr, Daniel L. Creedon, Yaohui Fan, Mikhail Kostylev, and Michael E. Tobar. High-cooperativity cavity qed with magnons at microwave frequencies. *Phys. Rev. Applied*, 2:054002, Nov 2014.

[16] Yutaka Tabuchi, Seiichiro Ishino, Toyofumi Ishikawa, Rekishu Yamazaki, Koji Usami, and Yasunobu Nakamura. Hybridizing ferromagnetic magnons and microwave photons in the quantum limit. *Phys. Rev. Lett.*, 113:083603, Aug 2014.

[17] Xufeng Zhang, Chang-Ling Zou, Liang Jiang, and Hong X. Tang. Strongly coupled magnons and cavity microwave photons. *Phys. Rev. Lett.*, 113:156401, Oct 2014.

[18] Hans Huebl, Christoph W. Zollitsch, Johannes Lotze, Fredrik Hocke, Moritz Greifenstein, Achim Marx, Rudolf Gross, and Sebastian T. B. Goennenwein. High cooperativity in coupled microwave resonator ferrimagnetic insulator hybrids. *Phys. Rev. Lett.*, 111:127003, Sep 2013.

[19] Xufeng Zhang, Na Zhu, Chang-Ling Zou, and Hong X. Tang. Optomagnonic whispering gallery microresonators. *Phys. Rev. Lett.*, 117:123605, Sep 2016.

[20] J. A. Haigh, S. Langenfeld, N. J. Lambert, J. J. Baumberg, A. J. Ramsay, A. Nunnenkamp, and A. J. Ferguson. Magneto-optical coupling in whispering-gallery-mode resonators. *Phys. Rev. A*, 92:063845, Dec 2015.

[21] A. Osada, R. Hisatomi, A. Noguchi, Y. Tabuchi, R. Yamazaki, K. Usami, M. Sadgrove, R. Yalla, M. Nomura, and Y. Nakamura. Cavity optomagnonics with spin-orbit coupled photons. *Phys. Rev. Lett.*, 116:223601, Jun 2016.

[22] V. Baltz, A. Manchon, M. Tsoi, T. Moriyama, T. Ono, and Y. Tserkovnyak. Antiferromagnetic spintronics. *Rev. Mod. Phys.*, 90:015005, Feb 2018.

[23] Christian Tzschaschel, Kensuke Otani, Ryugo Iida, Tsutomu Shimura, and Takuya Satoh. Ultrafast optical excitation of coherent magnons in antiferromagnetic nio. *Physical Review B*, 95:174407, 01 2017.

[24] Alireza Qaiumzadeh, Lars A. Kristiansen, and Arne Brataas. Controlling chiral domain walls in antiferromagnets using spin-wave helicity. *Phys. Rev. B*, 97:020402, Jan 2018.

[25] A. N. Bogdanov, U. K. Rößler, M. Wolf, and K.-H. Müller. Magnetic structures and reorientation transitions in noncentrosymmetric uniaxial antiferromagnets. *Phys. Rev. B*, 66:214410, Dec 2002.

[26] Andrzej Janutka and Przemyslaw Gawronski. Structure of magnetic domain wall in cylindrical microwire. *IEEE Transactions on Magnetics*, 51, 07 2014.

[27] Cyrill B. Muratov, Valeriy V. Slastikov, Alexander G. Kolesnikov, and Oleg A. Tretiakov. Theory of the dzyaloshinskii domain-wall tilt in ferromagnetic nanostrips. *Phys. Rev. B*, 96:134417, Oct 2017.

[28] Jasmin Graf, Hannes Pfeifer, Florian Marquardt, and Silvia Viola Kusminskiy. Cavity optomagnonics with magnetic textures: Coupling a magnetic vortex to light. *Physical Review B*, 98, 12 2018.

[29] Hans-Benjamin Braun, Jiri Kulda, Bertrand Roessli, Dirk Visser, Karl Krämer, Hans-Ulrich Güdel, and Peter Böni. Emergence of soliton chirality in a quantum antiferromagnet. *Nat Phys*, 1, 11 2005.

[30] Yoji Ichiraku, Rikuho Takeda, Seiya Shimono, Masaki Mito, Yoshiki Kubota, Katsuya Inoue, and Yusuke Kato. Magnetic phase diagram and chiral soliton phase of chiral antiferromagnet [nh4][mn(hcoo)3]. *Journal of the Physical Society of Japan*, 88(9):094710, 2019.

[31] Alexei Kolezhuk. Solitons with internal degrees of freedom in 1d heisenberg antiferromagnets. *Physical review letters*, 74:1859–1862, 04 1995.

[32] I. G. Bostrem, Jun-ichiro Kishine, and A. S. Ovchinnikov. Transport spin current driven by the moving kink crystal in a chiral helimagnet. *Phys. Rev. B*, 77:132405, Apr 2008.

[33] Jun-ichiro Kishine, I. G. Bostrem, A. S. Ovchinnikov, and Vl. E. Sinitsyn. Coherent sliding dynamics and spin motive force driven by crossed magnetic fields in a chiral helimagnet. *Phys. Rev. B*, 86:214426, Dec 2012.

[34] Gen Tatara, Hiroshi Kohno, and Junya Shibata. Microscopic approach to current-driven domain wall dynamics. *Physics Reports*, 468(6):213–301, 2008.

[35] Erlend G. Tveten, Alireza Qaiumzadeh, O. A. Tretiakov, and Arne Brataas. Staggered dynamics in antiferromagnets by collective coordinates. *Phys. Rev. Lett.*, 110:127208, Mar 2013.

[36] Djemoui Bouzidi and Harry Suhl. Motion of a bloch domain wall. *Phys. Rev. Lett.*, 65:2587–2590, Nov 1990.

[37] O. A. Tretiakov, D. Clarke, Gia-Wei Chern, Ya. B. Bazaliy, and O. Tchernyshyov. Dynamics of domain walls in magnetic nanostrips. *Phys. Rev. Lett.*, 100:127204, Mar 2008.

[38] Erlend Tveten, Tristan Müller, Jacob Linder, and Arne Brataas. The intrinsic magnetization of antiferromagnetic textures. *Physical Review B*, 93, 06 2015.

[39] Erlend Tveten, Alireza Qaiumzadeh, and Arne Brataas. Antiferromagnetic domain wall motion induced by spin waves. *Physical review letters*, 112:147204, 04 2014.

[40] Se Kwon Kim, Yaroslav Tserkovnyak, and Oleg Tchernyshyov. Propulsion of a domain wall in an antiferromagnet by magnons. *Phys. Rev. B*, 90:104406, Sep 2014.

[41] D. Bang, Pham Van Thach, and H. Awano. Current-induced domain wall motion in antiferromagnetically coupled structures: Fundamentals and applications. *Journal of Science: Advanced Materials and Devices*, 3:389–398, 2018.

[42] Dany Lachance-Quirion, Yutaka Tabuchi, Arnaud Gloppe, Koji Usami, and Yasunobu Nakamura. Hybrid quantum systems based on magnonics. *Applied Physics Express*, 12(7):070101, jun 2019.

[43] Igor Proskurin, Alexander S. Ovchinnikov, Jun-ichiro Kishine, and Robert L. Stamps. Cavity optomechanics of topological spin textures in magnetic insulators. *Phys. Rev. B*, 98:220411, Dec 2018.

[44] Ole Knudsen. The faraday effect and physical theory, 1845-1873. *Archive for History of Exact Sciences*, 15(3):235–281, 1976.

[45] J. P. van der Ziel, P. S. Pershan, and L. D. Malmstrom. Optically-induced magnetization resulting from the inverse faraday effect. *Phys. Rev. Lett.*, 15:190–193, Aug 1965.

[46] Teo Conzelmann, Severin Selzer, and Ulrich Nowak. Domain walls in antiferromagnets: The effect of dzyaloshinskii–moriya interactions. *Journal of Applied Physics*, 127(22):223908, 2020.

[47] N. Papanicolaou. Dynamics of domain walls in weak ferromagnets. *Phys. Rev. B*, 55:12290–12308, May 1997.

[48] N. Papanicolaou. Antiferromagnetic domain walls. *Phys. Rev. B*, 51:15062–15073, Jun 1995.

[49] Jin Lan, Weichao Yu, and Jiang Xiao. Antiferromagnetic domain wall as spin wave polarizer and retarder. *Nature Communications*, 8, 06 2017.

[50] B. A. Ivanov. Spin dynamics of antiferromagnets under action of femtosecond laser pulses (review article). *Low Temperature Physics*, 40(2):91–105, 2014.

[51] J. M. D. Coey. *Magnetism and Magnetic Materials*. Cambridge University Press, 2010.

[52] Hans-Benjamin Braun. Fluctuations and instabilities of ferromagnetic domain-wall pairs in an external magnetic field. *Phys. Rev. B*, 50:16485–16500, Dec 1994.

[53] Jasper Vandermeulen, Ben Wiele, Arne Vansteenkiste, Bartel Waeyenberge, and Luc Dupré. A collective coordinate approach to describe magnetic domain wall dynamics applied to nanowires with high perpendicular anisotropy. *Journal of Physics D: Applied Physics*, 48:035001, 01 2015.

[54] Andrei Kirilyuk, Alexey Kimel, and Theo Rasing. Ultrafast optical manipulation of magnetic order. *Reviews of Modern Physics*, 82:2731–2784, 07 2010.

[55] T. S. Parvini, V. A. S. V. Bittencourt, and Silvia Viola Kusminskiy. Antiferromagnetic cavity optomagnonics. *Phys. Rev. Research*, 2:022027, May 2020.

[56] Silvia Kusminskiy. *Quantum Magnetism, Spin Waves, and Light*. Springer, 07 2018.

[57] M. Peck, Yung Huh, R. Skomski, Rui Zhang, Parashu Kharel, M. Allison, David Sellmyer, and M. Langell. Magnetic properties of nio and (ni, zn)o nanoclusters. *Journal of Applied Physics*, 109, 03 2011.

[58] Hisamoto Kondoh. Antiferromagnetic Resonance in NiO in Far-infrared Region. *Journal of the Physical Society of Japan*, 15(11):1970–1975, November 1960.

[59] Daniel Stancil and A. Prabhakar. *Spin Waves: Theory and Applications*. 01 2009.

Connection between the chapter 2 and Chapter 3

A major connecting factor between the two papers included in this thesis is the phenomenon of level attraction, which is one of the signatures of cavity magnonic systems. As demonstrated in Ref. [1], level attraction can be realized when there is an instability in a system of two coupled oscillators.

In the analytical studies of cavity magnonics described in chapter 2, a Hamiltonian formalism has been used to describe a magnon-photon system as a set of harmonic oscillators. The Hamiltonian of the system consists of the magnonic Hamiltonian, the photonic Hamiltonian, and the coupling between the two. The coupling mechanism is the inverse Faraday effect, which introduces non-linearity into the system. This creates an effective magnetic field within the material due to the interaction of the circularly polarized field with the electrons' spin. To remove the time dependence in the Hamiltonian of the system, we switched to a frame rotating at the laser frequency. Switching to the rotating frame resulted in a detuning term, which is a difference between the cavity photon frequency and the drive frequency. The detuning parameter is either positive ($\Delta > 0$) or negative ($\Delta < 0$) depending on the region of interaction. The regions of positive and negative detuning correspond to the regions of repulsion and attraction, respectively.

The presence of non-linearity in the coupled system can create conditions for level attraction. A strong driving field can drive a non-linear magnetic response known as a P-mode in some systems. In Chapter 3, an example is discussed with driving by a time-periodic circularly polarized field. When perturbations are introduced in the system, we have excitations about a steady state. These excitations form two sidebands with respect to the driving frequency. The sideband with frequency below the driving frequency corresponds to level attraction while that above the driving frequency

corresponds to level repulsion, similar to the result in chapter 2.

As in chapter 2, the starting point of the analytical calculations in chapter 3 is a description of the system as a set of harmonic oscillators. This approach helped to study the dynamics of the coupled system, allowing for the derivation of the equations of motion for the coupled system. The formalism in chapter 3 opened up the possibility of replacing the equations of motion with a numerical scheme, which allows us to extract from micromagnetics the dynamic response of the system.

Bibliography

[1] N. R. Bernier, L. D. Tóth, A. K. Feofanov, and T. J. Kippenberg. Level attraction in a microwave optomechanical circuit. *Phys. Rev. A*, 98:023841, Aug 2018.

Chapter 3

Mode attraction in Floquet systems with memory: application to magnonics

Level attraction is a type of mode hybridization in open systems where instead of forming a hybridization gap, the energy spectrum of two modes coalesce in a region bounded by exceptional points. We demonstrate that this phenomenon can be realized in a Floquet system with memory, which appears in describing linear excitations in a nonlinear driven system with a limit cycle. Linear response of the system in this state is different from its response near thermodynamic equilibrium. We develop a general formalism and provide an example in the context of cavity magnonics, where we show that magnetic excitations in systems driven far from the equilibrium may show level attraction with cavity photons. Our approach works equally well for quantum and semiclassical magnetic dynamics. The theory is formulated so that it can be used in combination with micromagnetic simulations to explore a wide range of experimentally interesting systems.

3.1 Introduction

Excitations around dynamic steady states in open nonlinear systems away from the equilibrium can show features that cannot be observed near the ground state, and can be broadly understood

[1]DOI: https://doi-org.uml.idm.oclc.org/10.1103/PhysRevB.105.224420

in terms of non-Hermitian physics [1, 2]. An example is level attraction as recently demonstrated in a dissipative magnon-polariton microwave cavity [3]. This is a dynamic regime characterized by a region where the energy levels of the interacting cavity system coalesce [4]. The appearance of exceptional points delineating the attraction is a non-Hermitian phenomenon [5, 6] that can take place in driven systems for some types of dissipation [7, 8, 9]. The energy levels near the exceptional points are sensitive to manipulation through external parameters and are potentially useful for mode control and sensing [10, 11, 12].

Mode attraction and exceptional points have been studied extensively in magnonics both theoretically and experimentally [13, 14, 15, 16, 17, 18, 19, 20, 21, 22, 23, 24]. Theoretical description has been based largely on various models of coupled oscillators borrowed from cavity electrodynamics [25, 26, 27, 28] with additional non-Hermitian mechanisms [17, 18] such as dissipative coupling [29, 30] and nonlocal interactions [31, 32].

Recently Floquet states for linear excitations around equilibrium in an open cavity magnonic system have been realized experimentally [33]. It has been demonstrated that higher order Floquet bands may contribute significantly to the cavity reflection spectrum in the Floquet ultrastrong coupling regime.

The main focus of the present paper is on magnonics around non-linear steady states away from equilibrium. This allows us to realize level attraction, which does not appear in a linear Floquet cavity system. We show that dynamics of the system can be understood on the basis of a generalized Floquet theorem for non-Markovian kinetic equations [34, 35, 36, 37]. Regions of stability and instability, determined by the Floquet index of the system, can be associated with mode repulsion and attraction between the system and the excited states of the reservoir. This approach is equally applicable to quantum and semi-classical dynamics, and can be used in combination with numeric methods. Our theory is quite general, and can be applied to a variety of magnetic and non-magnetic systems.

In order to illustrate application of our theory, we demonstrate how the Floquet formalism can be used in magnonics by considering a microwave cavity loaded with a driven magnetic specimen. This situation has been recently realized experimentally in a microwave cavity, where a magnetic specimen has been probed and driven out of equilibrium using separate ports [17, 18]. In this system, the cavity

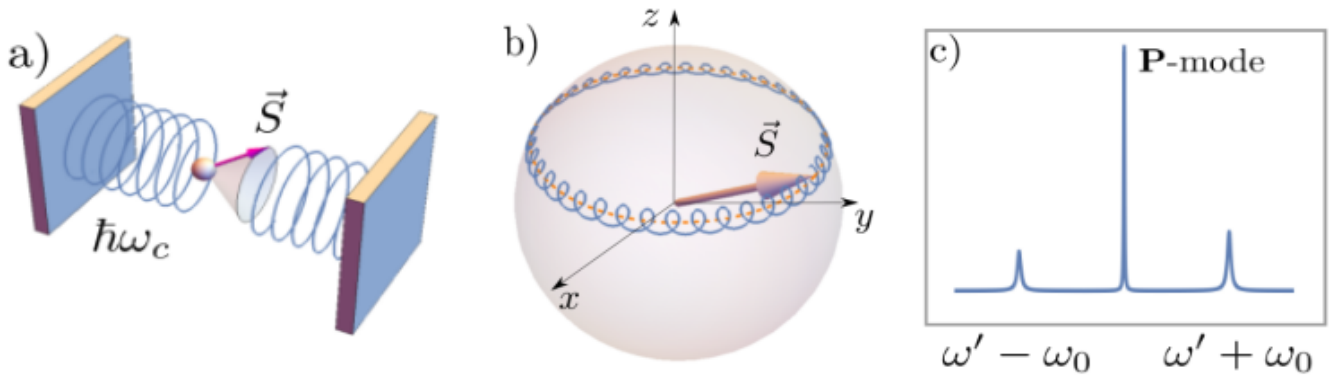

Figure 3.1: (a) A small magnetic specimen inside a microwave cavity resonator. (b) Schematic picture of an excitation around a **P**-mode stationary trajectory of spin precession (dashed line), and (c) the corresponding Fourier spectrum showing the **P**-mode at the frequency of the driving field ω', and two side bands with the frequencies $\omega' \pm \omega_0$.

photons serve as probes that can read out magnetization dynamics. Details of this process can be described using a generalized susceptibility [38] given by a nonequilibrium Green function [39, 40, 41].

Far from thermodynamic equilibrium, nonlinear magnetization dynamics in systems that have uniaxial rotation symmetry can be characterized by steady state trajectories known as **P**-modes [42]. The number of **P**-modes is described by the Poincaré-Bendixson theorem [43] and their stability depends on details of microscopic interactions. Stable **P**-modes provide a steady state about which elementary excitations can exists. These excitations have finite lifetime, and form two side bands with respect to the driving frequency. This feature has been used recently for nutation spectroscopy in nonlinear ferromagnetic resonance [44].

We show that in **P**-mode cavity magnonics a hybridization between cavity photons and excitations around the **P**-mode can occur, which depends on whether the cavity resonance is tuned to the lower or upper side band. If the phase of the resonance in the lower band is shifted by π with respect to the upper band level attraction instead of repulsion appears.

Our paper is organized as follows. In Sec. 3.2 we consider a general formalism for a probe system in contact with a driven reservoir. This formalism is applied to a cavity magnonic systems in Sec. 3.3. Section 3.4 is reserved for the discussion of results, and Sec. 3.5 is for the conclusions.

3.2 General formalism

We begin by outlining a theory for periodically driven systems. In the magnonic experiment described above, the cavity photon system is the probe, and is characterized by a density matrix $\hat{\rho}(t)$. The probe is assumed to be weakly coupled to the driven system (i. e. the magnetic sample loading the cavity), which is characterized by the density matrix $\hat{\rho}_r(t)$. The total Hamiltonian of the interacting system is given by

$$\hat{H}^t_{\text{tot}} = \hat{H}^t_s + \hat{H}^t_r + \hat{H}^t_i, \tag{3.1}$$

where the first term is the Hamiltonian of the probe, the second corresponds to the driven system and the last is the interaction part. The index t indicates that each term can be explicitly time-dependent.

The total interacting system is characterized by the density matrix $\hat{\rho}_{\text{tot}}(t)$, and its dynamics is described by the Liouville equation

$$\left(\frac{\partial}{\partial t} + i\mathcal{L}^t_s + i\mathcal{L}^t_r + i\mathcal{L}^t_i\right)\hat{\rho}_{\text{tot}}(t) = -\varepsilon\left(\hat{\rho}_{\text{tot}}(t) - \hat{\rho}(t)\hat{\rho}_r(t)\right), \tag{3.2}$$

where $i\mathcal{L}^t_\alpha \ldots = \frac{1}{i\hbar}[\ldots, \hat{H}^t_\alpha]$ $(\alpha = s, r, i)$ denote the Liouville operators for the probe, driven system and the interaction part correspondingly. We assume that the probe and the driven system are uncoupled at $t \to -\infty$, so that the term on the right hand side is the boundary condition with $\varepsilon \to 0^+$, which breaks time reversal symmetry [39].

The density matrix of the probe system, which in this approach is treated as a reservoir, is obtained from $\hat{\rho}_{\text{tot}}(t)$ by taking a partial trace over the states of the driven system, $\hat{\rho}(t) = \text{Tr}_r\, \hat{\rho}_{\text{tot}}(t)$. The time-evolution of $\hat{\rho}_r(t)$ is teated as independent from dynamics of the probe system, and is described by the separate Liouville equation

$$\frac{\partial \hat{\rho}_r(t)}{\partial t} + i\mathcal{L}^t_r\hat{\rho}_r(t) = 0. \tag{3.3}$$

A closed master equation for $\hat{\rho}(t)$ can be derived using the methods of relaxation dynamics in open dissipative systems [39]. We outline the most important steps in Appendix D. For weakly coupled

systems, the master equation for $\hat{\rho}(t)$ has the following form

$$\frac{\partial\hat{\rho}(t)}{\partial t}+\frac{1}{i\hbar}[\hat{\rho}(t),\hat{H}_s^t]=\frac{1}{(i\hbar)^2}\int_{-\infty}^{t}dt'e^{-\varepsilon(t-t')}\mathrm{Tr}_r[\hat{H}_i^t,[\hat{H}_i^{t'}(t,t'),\hat{\rho}(t,t')\hat{\rho}_r(t)]], \tag{3.4}$$

where $\hat{H}_i^{t'}(t,t')=\hat{U}_{tt'}\hat{H}_i^{t'}\hat{U}_{tt'}^{-1}$ and $\hat{\rho}(t,t')=\hat{U}_{tt'}\hat{\rho}(t')\hat{U}_{tt'}^{-1}$ are defined with the evolution operator

$$\hat{U}_{tt'}=\mathcal{T}\exp\left[-\frac{i}{\hbar}\int_{t'}^{t}d\tau\left(\hat{H}_s^{\tau}+\hat{H}_r^{\tau}\right)\right]. \tag{3.5}$$

Here $\mathcal{T}$ denotes the time-ordering operator and the trace in the right hand side of Eq. (3.4) is with respect to the Hilbert space of the driven system.

In the Markov's approximation, $\hat{U}_{tt'}\hat{\rho}(t')\hat{U}_{tt'}^{-1}\approx\hat{\rho}(t)$, and Eq. (3.4) reduces to the Lindblad master equation [45]. It is important to keep track of memory effects, which later allow us to calculate the energy spectrum of the interacting system.

3.2.1 Kinetic equation for the probe system

The right hand side of Eq. (3.4) is simplified if the interaction part is taken as a product of operators, $\hat{H}_i=\hat{a}\hat{F}+\hat{a}^{\dagger}\hat{F}^{\dagger}$, where $\hat{a}$ and $\hat{a}^{\dagger}$ characterize the probe system, and $\hat{F}$ and $\hat{F}^{\dagger}$ act entirely in the space of the driven system. In the case when $\hat{a}$ and $\hat{a}^{\dagger}$ satisfy a boson commutation relation, Eq. (3.4) yields the following non-Markovian kinetic equation for the field amplitude of the probe system $\langle\hat{a}\rangle^t=\mathrm{Tr}(\hat{a}\hat{\rho}(t))$

$$i\hbar\frac{d\langle\hat{a}\rangle^t}{dt}+\langle[\hat{H}_s^t,\hat{a}]\rangle^t-\int_{-\infty}^{t}dt'G(t,t')\langle\hat{a}\rangle^{t'}=\langle\hat{F}^{\dagger}(t)\rangle_r, \tag{3.6}$$

where the memory kernel is given by the nonequilibrium retarded Green function [39, 46, 41]

$$G(t,t')=\frac{1}{i\hbar}e^{-\varepsilon(t-t')}\theta(t-t')\langle[\hat{F}^{\dagger}(t),\hat{F}(t')]\rangle_r. \tag{3.7}$$

Here the operators $\hat{F}^{\dagger}(t)$ and $\hat{F}(t)$ are in the Heisenberg picture and satisfy the equation of motion $i\hbar\partial_t\hat{F}=[\hat{F},\hat{H}_r^t]$ with the time-dependent Hamiltonian. The average in Eq. (3.7), $\langle\ldots\rangle_r\equiv\mathrm{Tr}_r[\ldots\hat{\rho}_r(-\infty)]$, is taken with respect to the density matrix of the driven system at the initial time

moment, $\hat{\rho}_r(-\infty)$. The last term in Eq. (3.7) is the driving inherited from the dynamics of the reservoir.

3.2.2 Semi-classical periodically driven systems

For a semi-classical nonlinear system near the stable limit cycle regime of motion with period T, the memory kernel in Eq. (3.7) is bi-periodic in time, such that $G(t+T,t'+T) = G(t,t')$. To illustrate this, we expand the operators in the interaction Hamiltonian near the steady state trajectory using $\hat{F}(t) = F_{\rm cl}(t) + \delta\hat{F}(t)$ [46], where the first term describes the semi-classical solution of the equations of motion, and $\delta\hat{F}(t)$ is a perturbation. Requiring that the elementary excitations around the steady state be characterized by one degree of freedom, we expand $\delta\hat{F}(t)$ around $F_{\rm cl}(t)$ as

$$\delta\hat{F}(t) = \left(\frac{\partial F_{\rm cl}}{\partial b}\right)_t \hat{b}(t) + \left(\frac{\partial F_{\rm cl}}{\partial b}\right)_t \hat{b}^\dagger(t), \tag{3.8}$$

taken to the first order in terms of the boson operators $b(t)$ and $b^\dagger(t)$, which describe the excitations. In the linear approximation, $b(t)$ and $b^\dagger(t)$ satisfy equations of motion with time-periodic coefficients. These can be characterized by a Floquet solution $(\hat{b}(t),\hat{b}^\dagger(t))^T = \hat{A}e^{i\nu t}F_\nu(t) + \hat{B}e^{-i\nu t}F^*_\nu(t)$, where ν is the Floquet index and $F_\nu(t)$ is periodic in time with period T. The coefficients $\hat{A}$ and $\hat{B}$ are determined from the initial conditions $\hat{b}(0) = \hat{b}$ and $\hat{b}^\dagger(0) = \hat{b}^\dagger$.

By substituting $b(t)$ and $b^\dagger(t)$ into the memory kernel (3.7), we find $G(t,t') \sim i[K_{1\nu}(t)K^*_{1\nu}(t')$ $\exp(i\nu(t-t')) - K_{2\nu}(t)K^*_{2\nu}(t')\exp(-i\nu(t-t'))]$ $(t > t')$, where $K_{i\nu}(t)$ $(i = 1, 2)$ is a periodic function whose explicit form depends on the details of the limit cycle and interactions. This form of the memory kernel is manifestly bi-periodic in time so that the kinetic equation (3.6) falls under the conditions of the generalized Floquet theorem [34] and can be analyzed by methods of embedding [35] and harmonic balance [37]. This memory kernel can be also interpreted as a linear susceptibility around the nonlinear steady state in the Floquet system, similar to Ref. [38].

By applying the generalized Floquet theorem [34, 35] to the homogeneous equation associated with Eq. (3.6), we find that dynamics the probe system can be characterized by a Floquet index λ, which depends on parameters of the driven system and interactions [37]. If we take the probe system in a form of Harmonic oscillator, $\hat{H}_s = \hbar\omega_c\hat{a}^\dagger\hat{a}$ with the frequency ω_c, the Floquet index $\lambda = \lambda(\omega_c,\nu)$

becomes a function of ν and ω_c, and can be considered as the hybridized spectrum of the interacting system.

In the absence of driving, when ν is the frequency of the excitations around equilibrium, hybridization between two energy levels leads to a level repulsion, so that $\lambda(\omega_c, \nu)$ remains real outside the hybridization gap. For a driven Floquet system it is possible, however, that λ may become complex even if the systems are characterized by real ω_c and ν in absence of interaction.

To illustrate this idea, let us consider the case when time-dependence of the coefficients $K_{i\nu}(t)$ in the memory kernel can be approximated by a single harmonic, $K_{i\nu}(t) = K_{i\nu}e^{i\omega' t}$, where ω' is associated with the driving frequency. As we show later, this case is realized for a magnetic oscillator driven with the circularly polarized field. The Green function in this case becomes a function of $t-t'$, and has the following form

$$G(t-t') = \frac{e^{i\varepsilon(t-t')}}{i\hbar\nu}\theta(t-t')\left(|K_{1\nu}|^2 e^{i(\omega'+\nu)(t-t')} - |K_{2\nu}|^2 e^{i(\omega'-\nu)(t-t')}\right), \tag{3.9}$$

which shows two resonances with the negative and positive frequencies with respect to reference frequency ω'. Note that these resonances enter with opposite signs that represents an additional π phase difference.

The energy spectrum of the coupled system is found by Fourier transforming Eq. (3.6), which leads to $\omega - \omega_c = G(\omega)$, where $G(\omega) = \int_{-\infty}^{\infty} d\tau \exp(-i\omega\tau)G(\tau)$. The first term in Eq. (3.9) describes level hybridization between ω_c and $\omega' + \nu$ with the hybridization gap proportional to $|K_\nu|$. The second term has $\omega' - \nu$ and corresponds to level attraction when ω' is greater that ν.

3.3 Application to magnonics

For magnonics, we associate $\hat{H}_s$ with a system of cavity photons, and ω_c with the resonant frequency of cavity. The photons interact with a spin system, which we model as a driven reservoir as above. Spin dynamics of the reservoir are described semi-classically. The interaction between the photon and spin system is assumed to be of the form of a dipolar interaction, $\hat{H}_i = g(\hat{a}\hat{S}^{(+)} + \hat{a}^\dagger\hat{S}^{(-)})$ where g is the interaction constant. The operators $\hat{S}^{(\pm)} = \hat{S}^x \pm \hat{S}^y$ denote the circular components of the spin and $\hat{a}$ ($\hat{a}^\dagger$) is the photon annihilation (creation) operator. The weak coupling assumption in

Eq. (3.6) means that interaction with cavity photons does not affect the steady state magnetization dynamics. Consequently, g should be small compared to the characteristic energy of the ferromagnetic resonance.

The kinetic equation in Eq. (3.6) works equally well for quantum and classical dynamics of the reservoir. In the latter case, one has to replace the commutator with the Poisson bracket, $(i\hbar)^{-1}[\hat{F}^{\dagger}(t), \hat{F}(t)] \to \{F^{*}(t), F(t)\}$ [39], where $F(t)$ and $F^{*}(t)$ are functions of canonical variables, and the trace over the Hilbert space becomes an integral over phase space.

For a block spin system, semi-classical dynamics is described by the Lagrangian $\mathcal{L} = \sum_i S\cos\theta_i \partial\phi_i/\partial t - \mathcal{H}_m$ where the first term is the Berry phase expressed in terms of the azimuthal angle, ϕ_i, and polar angle, θ_i, and the last term is the spin Hamiltonian. The Poisson bracket for the two block spin components is defined as [47]

$$\left\{S^{\alpha}(t), S^{\beta}(t')\right\} = -\frac{1}{S\sin\theta_1}\left(\frac{\partial S^{\alpha}(t)}{\partial\phi_1}\frac{\partial S^{\beta}(t')}{\partial\theta_1} - \frac{\partial S^{\alpha}(t)}{\partial\theta_1}\frac{\partial S^{\beta}(t')}{\partial\phi_1}\right), \tag{3.10}$$

where the derivatives are taken with respect to $\phi_1 = \phi(t_1)$ and $\theta_1 = \theta(t_1)$ at the initial time t_1 and are treated as the initial conditions for the spin trajectory $S(t) = S(t;\phi_1,\theta_1)$. For $t = t'$, this expression is evaluated as $\{S^{\alpha}, S^{\beta}\} = \epsilon_{\alpha\beta\gamma}S^{\gamma}$, which is a semi-classical analogue of the spin commutation relations.

3.3.1 Semi-classical spin driven by the circularly polarize magnetic field

The spin dynamics is calculated from the Landau-Lifshitz-Gilbert equation

$$\frac{\partial S}{\partial t} = -\gamma S \times B_{\text{eff}} + \frac{\alpha}{M_s} S \times \frac{\partial S}{\partial t}, \tag{3.11}$$

where γ is the gyromagnetic ratio, α is the Gilbert damping constant, M_s is the saturation magnetization, and $B_{\text{eff}} = -\delta\mathcal{H}_m/\delta S$ is the effective field. Here, we consider uniform precession of a single block macro-spin driven with a circularly polarized magnetic field in a situation where the rotation symmetry along the z axis is preserved. This configuration supports existence of the time-harmonic **P**-modes and prevents the onset of a chaotic regime [42].

We transform the equation of motion in Eq. (3.11) to dimensionless form by introducing the

following notations

$$m = \frac{S}{M_s}, \quad h_{\text{eff}} = \frac{B_{\text{eff}}}{\mu_0 M_s}, \quad \tilde{t} = \gamma \mu_0 M_s t, \tag{3.12}$$

where μ_0 is the vacuum permeability, and $\tilde{t}$ is the dimensionless time variable. In the dimensionless units, the Eq. (3.11) becomes $\dot{m} = -m \times h_{\text{eff}} + \alpha m \times \dot{m}$, where we identify four contributions to the effective field, $h_{\text{eff}} = h_a + h_M + h_{\text{AN}} + h_{\text{ex}}$. The first is the applied field, which contains a static field along the z axis and the transverse dynamic driving field, $h_a = h_{az}\hat{z} + h_\perp(t)$. The second term is the demagnetizing field that preserves the rotation symmetry along z, $h_M = -N_\perp m_\perp - N_z m_z \hat{z}$. The third term is a uniaxial anisotropy field along the z direction, $h_{\text{AN}} = 2K_1 m_z \hat{z}/(\mu_0 M_s^2)$ with K_1 being the anisotropy constant. And finally, since we only consider dynamics of uniformly magnetized medium, the exchange field h_{ex} vanishes. The total effective field is written as $h_{\text{eff}} = h_\perp(t) + (h_{az} + \varkappa m_z)\hat{z}$ where $\varkappa = 2K_1/(\mu_0 M_s^2) + N_\perp - N_z$ [42]. The physical fields are $B_\perp = \mu_0 M_s h_\perp$ and $B_z = \mu_0 M_s h_{az}$.

The equations of motion take the most simple form in a frame of reference co-rotating with the driving field [48]. We take the driving field as $h_\perp(t) = h_{a\perp}(\cos\omega' t, \sin\omega' t, 0)$, and use the following parametrization for the magnetization, $m = [\cos(\omega' t - \phi)\sin\theta, \sin(\omega' t - \phi)\sin\theta, \cos\theta]$, where $\phi = \phi(t)$ and $\theta = \theta(t)$ are dynamic variables. In this parametrization, from Eq. (3.11) we obtain the following system of autonomous differential equations [43] on the surface of a sphere [42]

$$\dot{\theta} + \alpha \sin\theta \dot{\phi} = \varkappa \left[b_\perp \sin\phi - \Omega \sin\theta \right], \tag{3.13}$$

$$\alpha \dot{\theta} + \sin\theta \dot{\phi} = \varkappa \left[b_\perp \cos\phi \cos\theta - \sin\theta \left(b_z + \cos\theta \right) \right], \tag{3.14}$$

where $b_\perp = h_{a\perp}/\varkappa$, $b_z = (h_{az} - \tilde{\omega}')/\varkappa$, $\Omega = \alpha\tilde{\omega}'/\varkappa$, and $\tilde{\omega}' = \omega'/(\gamma\mu_0 M_s)$ denotes the dimensionless frequency.

The static solution of these equations can be conveniently parameterized as [42]

$$b_z = m_z (v - 1), \tag{3.15}$$

$$b_\perp^2 = \left(1 - m_z^2\right)\left(\Omega^2 + v^2\right). \tag{3.16}$$

where $m_z = \cos\theta$, and $v = \Omega \cot\phi$. In the original frame, these solutions correspond to uniform magnetization precession with frequency ω', and are known as "**P**-modes". Stability of the **P**-modes

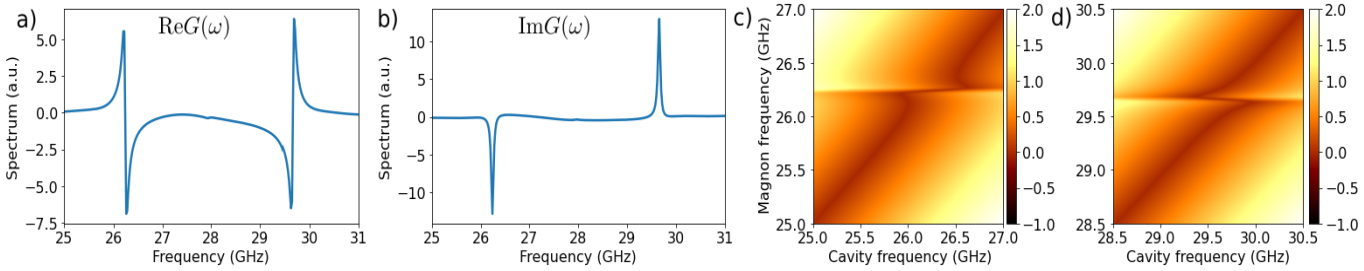

Figure 3.2: Real (a) and imaginary (b) parts of $G(\omega)$ obtained in micromagnetic simulations for a spherical particle with $B_z = 1$ T, $B_\perp = 0.01$ T, and $\omega'/2\pi = 27.95$ GHz. Two bands correspond to the excitations with the frequencies $\omega' \pm \omega_0$. The density plots for level attraction near $\omega' - \omega_0$ (c) and repulsion near $\omega' + \omega_0$ (d) are obtained from the equation $\omega - \omega_c = \mathrm{Re}G(\omega)$ with $\tilde{g}/2\pi = 35$ MHz.

has been studied in Ref. [42].

In the case of $\alpha = 0$ and $\varkappa = 0$, these equations reduce to $\sin\phi = 0$, and $\tan\theta = b_\perp/b_z$, which describe the magnetization aligned along the direction of the stationary effective field $b_\perp\hat{x} + b_z\hat{z}$ in the co-rotating frame [48].

Linear excitations around a stable **P**-mode can described with expansions $\theta(t) = \theta_0 + \delta\theta(t)$ and $\phi(t) = \phi_0 + \delta\phi(t)$, which leads to the following equations of motion in the co-rotating frame

$$\begin{pmatrix} \delta\dot{\theta} \\ \delta\dot{\phi} \end{pmatrix} = \frac{\varkappa}{1+\alpha^2} \begin{pmatrix} \alpha(1-m_z^2) - A & B\sin\theta_0 \\ \dfrac{1-m_z^2-B}{\sin\theta_0} & -A \end{pmatrix} \begin{pmatrix} \delta\theta \\ \delta\phi \end{pmatrix}, \tag{3.17}$$

where $A = \alpha v + \Omega m_z$ and $B = v - \alpha\Omega m_z$. From these equations of motion, we calculate the eigenfrequencies for linear excitations $\tilde{\lambda}_0 = -\tilde{\gamma}_0 \pm i\tilde{\omega}_0$, where $\tilde{\gamma}_0$ and $\tilde{\omega}_0$ are in the dimensionless units, e. g., $\tilde{\omega}_0 = \omega_0/(\gamma\mu_0 M_s)$. Here, ω_0 corresponds the same frequency with the physical dimension restored. These frequencies can be found a general form, but in order to avoid complicated expressions, we only present results in the absence of uniaxial anisotropy, i.e. $\varkappa \to 0$. This gives $\tilde{\gamma}_0 = \alpha[b_z/m_z + \tilde{\omega}' m_z]/(1+\alpha^2)$ and $\tilde{\omega}_0 = [b_z/m_z - \alpha^2\tilde{\omega}' m_z]/(1+\alpha^2)$. A general analysis is qualitatively the same and can be found in Appendix D.

Next, we apply our general formalism to the spin-photon interactions inside the microwave cavity. The Green function in Eq. (3.7) in this case is reduced to the spin-spin Poisson bracket $G(t,t') \sim \left\{S^{(-)}(t), S^{(+)}(t')\right\}$ $(t > t')$. In the linear approximation, this corresponds to a linear susceptibility around the **P**-mode. The corresponding Poisson bracket is calculated from Eq. (3.17) by solving the

equations of motion and taking the derivatives with respect to the initial conditions. This gives

$$\left\{S^{(-)}(t), S^{(+)}(t')\right\} = 2ig^2 e^{-(\gamma_0+i\omega')(t-t')}\left(\cos^4\frac{\theta_0}{2}e^{-i\omega_0(t-t')} - \sin^4\frac{\theta_0}{2}e^{i\omega_0(t-t')}\right), \tag{3.18}$$

in agreement with Eq. (3.9). This expression shows two side bands around ω' with the frequencies $\omega'+\omega_0$ and $\omega'-\omega_0$, which correspond to linear excitations around the **P**-mode. We note that this situation has been experimentally observed in Ref. [44]. When the spin is driven well out of equilibrium, the intensities of both side bands are the same, while close to thermodynamic equilibrium, $\theta_0 \approx 0$, the lower side band disappears as θ_0^4, and the upper side band evolves into the usual ferromagnetic resonance with the frequency γB_z.

3.3.2 Level attraction with cavity photons outside of equilibrium

Since the left hand side in Eq. (3.18) depends only on $t-t'$, the energy spectrum of the coupled spin-photon systems can be found by Fourier transforming Eq. (3.6) and solving the equation $\omega-\omega_c = \mathrm{Re}\, G(\omega)$, where $G(\omega) = \int_{-\infty}^{0} G(\tau)\exp(i\omega\tau)d\tau$. When the frequency of the cavity mode is close to the frequency of the lower side band, $\omega'-\omega_0$, the energy spectrum determined from this equation is given by

$$\omega^{(\pm)} = \frac{\omega_c+\Delta}{2} \pm \sqrt{\left(\frac{\omega_c-\Delta}{2}\right)^2 - \tilde{g}^2}, \tag{3.19}$$

where $\Delta = \omega'-\omega_0$ is the frequency of the lower side band and $\tilde{g} = g\sin^2(\theta_0/2)$ is the effective coupling parameter for the level attraction. Level attraction occurs in the region $(\omega_c-\Delta)^2 < 4\tilde{g}^4$. The coupling parameter is remormalized by the spin precession angle, and, therefore, strongly depends on the amplitude of the driving field. Close to thermodynamic equilibrium, the $\tilde{g}$ disappears as $\theta_0^2 \sim [\gamma B_\perp/(\gamma B_z-\omega')]^2$.

Strong enhancement of the effective coupling $\tilde{g}$ to the lower side-band with driving may be considered as an analogue of Floquet ultra-strong coupling in Ref. [33]. The main difference, however, from the Floquet states near equilibrium is that higher order harmonics are not excited even for strong driving. This allows for control of the coupling parameter through the steady state avoiding contributions from higher harmonic modes.

3.4 Numerical results and discussion

An advantage of considering semi-classical spin dynamics is that the nonequilibrium Green function for the spin components in Eq. (3.6) can be computed numerically from Eq. (3.10) for cases of practical interest. To illustrate, we performed micromagnetic simulations of macrospin dynamics using the MuMax3 package [49]. We considered dynamics of $16 \times 16 \times 16$ ellipsoid particle with the diameter of 100 nm, $M_s = 1 \times 10^6$ A/m, the exchange stiffness $A_{\rm ex} = 15 \times 10^{-12}$ J/m, and $\alpha = 9 \times 10^{-3}$ with enabled demagnetizing fields. The the static field $B_z = 1$ T has been applied along the z axis, and the circularly polarized microwave field with the frequency $\omega'/2\pi = 27.95$ GHz and $B_\perp = 0.01$ T has been applied perpendicular to z. The initial conditions for the **P**-mode have been identified from the stationary precession after a simulation time of 50 ns. The Poisson bracket has been evaluated by identifying the **P**-mode precession and estimating the derivatives in Eq. (3.10) numerically for the linear regime of deviation from the **P**-mode trajectory.

The results of simulations, presented in Fig. 3.2 (a) and (b), are in qualitative agreement with the analytical solution in Eq. (3.18) when demagnetizing fields are enabled in simulations. Without the demagnetizing field, the agreement becomes quantitative.

In the frequency domain, the Poisson bracket in Fig. 3.2 (a) shows two side bands around the driving frequency ω'. Note that the sign on the real part of the lower side band has been inverted with respect to the sign of the upper side band, which corresponds to π phase shift between two lines, in agreement with Eq. (3.18). We note that the coupling of the cavity photons to the excitations in the lower side band can be effectively described in terms of a non-Hermitian Hamiltonian, $\hat{\mathcal{H}} = \omega_c \hat{a}^\dagger \hat{a} + \Delta \hat{b}^\dagger \hat{b} + g_{\rm eff} e^{i\varphi}(a^\dagger b + a b^\dagger)$, with $\varphi = \pi/2$, and $\hat{b}$ and $\hat{b}^\dagger$ being magnon ladder operators. The possibility of such "dissipative" coupling has been discussed in a different context in Refs. [13, 18]. The density plots for attraction and repulsion, computed numerically from the equation $\omega - \omega_c = G(\omega)$, are shown in Fig. 3.2 (c) and (d) respectively where we used the coupling $\tilde{g}/2\pi = 35$ MHz for illustration purposes, which is within the same order as the coupling reported in Ref. [3].

Experimentally, a coupling between a microwave cavity field with externally driven magnetization has been realized in Refs. [17, 18]. These experiments demonstrated level attraction at substantially large driving field strengths. We think these results may be interpreted in terms of coupling of

microwave cavity photons with excitations above a nonlinear stationary state established by driving. In this case, the non-Hermitian coupling introduced in Refs. [17, 18] corresponds in our picture to the coupling to the lower side-band resonance in Eq. (3.18). However, a detailed discussion requires additional analysis since the driving field used in Refs. [17, 18] is linearly polarized.

3.5 Conclusion

We consider the possibility of level attraction in a coupled cavity magnon-polariton system, where a magnetic system is driven independently out of equilibrium. Using a master equation formalism, we demonstrate that this problem can be analyzed from the broader perspective of Floquet dynamics in systems with memory [34, 35]. From this point of view, level attraction can be interpreted as an instability developed as a result of interaction between excitations above a stationary driven magnetization **P**-mode and a probe system of cavity photons. We show that this instability develops when the cavity resonance is close to the frequency of the lower side band around the **P**-mode. The resulting interaction between two resonances can be interpreted using an effective non-Hermitian Hamiltonian with a dissipative coupling term [13, 18]. Level attraction quickly disappears when the reservoir approaches thermodynamic equilibrium. Our approach is promising for future analysis of level attraction in Floquet cavity magnonics [33] with non-equilibrium excited steady states such as discrete magnetic breather modes [50], and will be explained in future work.

Bibliography

[1] Hui Cao and Jan Wiersig. Dielectric microcavities: Model systems for wave chaos and non-hermitian physics. *Rev. Mod. Phys.*, 87:61–111, 01 2015.

[2] Yuto Ashida, Zongping Gong, and Masahito Ueda. Non-Hermitian physics. *Advances in Physics*, 69(3):249–435, 2020.

[3] M. Harder, Y. Yang, B. M. Yao, C. H. Yu, J. W. Rao, Y. S. Gui, R. L. Stamps, and C.-M. Hu. Level attraction due to dissipative magnon-photon coupling. *Phys. Rev. Lett.*, 121:137203, Sep 2018.

[4] N. R. Bernier, L. D. Tóth, A. K. Feofanov, and T. J. Kippenberg. Level attraction in a microwave optomechanical circuit. *Phys. Rev. A*, 98:023841, Aug 2018.

[5] W D Heiss. Exceptional points of non-hermitian operators. *Journal of Physics A: Mathematical and General*, 37(6):2455–2464, jan 2004.

[6] W. D. Heiss. The physics of exceptional points. *J. Phys. A*, 45(44):444016, Oct 2012.

[7] Ramy El-Ganainy, Konstantinos G. Makris, Mercedeh Khajavikhan, Ziad H. Musslimani, Stefan Rotter, and Demetrios N. Christodoulides. Non-Hermitian physics and PT symmetry. *Nature Physics*, 14(1):11–19, 2018.

[8] Yi-Pu Wang and Can-Ming Hu. Dissipative couplings in cavity magnonics. *Journal of Applied Physics*, 127(13):130901, 2020.

[9] M. Harder, B. M. Yao, Y. S. Gui, and C.-M. Hu. Coherent and dissipative cavity magnonics. *Journal of Applied Physics*, 129(20):201101, 2021.

[10] Weijian Chen, Şahin Kaya Özdemir, Guangming Zhao, Jan Wiersig, and Lan Yang. Exceptional points enhance sensing in an optical microcavity. *Nature*, 548(7666):192–196, 2017.

[11] Hossein Hodaei, Absar U Hassan, Steffen Wittek, Hipolito Garcia-Gracia, Ramy El-Ganainy, Demetrios N Christodoulides, and Mercedeh Khajavikhan. Enhanced sensitivity at higher-order exceptional points. *Nature*, 548(7666):187–191, 2017.

[12] Q. Zhong, J. Ren, M. Khajavikhan, D. N. Christodoulides, Ş. K. Özdemir, and R. El-Ganainy. Sensing with exceptional surfaces in order to combine sensitivity with robustness. *Phys. Rev. Lett.*, 122:153902, Apr 2019.

[13] Vahram L. Grigoryan and Ke Xia. Cavity-mediated dissipative spin-spin coupling. *Phys. Rev. B*, 100:014415, Jul 2019.

[14] J W Rao, C H Yu, Y T Zhao, Y S Gui, X L Fan, D S Xue, and C-M Hu. Level attraction and level repulsion of magnon coupled with a cavity anti-resonance. *New Journal of Physics*, 21(6):065001, jun 2019.

[15] Yi-Pu Wang, J. W. Rao, Y. Yang, Peng-Chao Xu, Y. S. Gui, B. M. Yao, J. Q. You, and C.-M. Hu. Nonreciprocity and unidirectional invisibility in cavity magnonics. *Phys. Rev. Lett.*, 123:127202, Sep 2019.

[16] C. H. Yu, Y. Yang, J. W. Rao, P. Hyde, Yi-Pu Wang, B. Zhang, Y. S. Gui, and C.-M. Hu. Spin number dependent dissipative coupling strength. *AIP Advances*, 9(11):115012, 2019.

[17] Isabella Boventer, Mathias Kläui, Rair Macêdo, and Martin Weides. Steering between level repulsion and attraction: broad tunability of two-port driven cavity magnon-polaritons. *New Journal of Physics*, 21(12):125001, 2019.

[18] Isabella Boventer, Christine Dörflinger, Tim Wolz, Rair Macêdo, Romain Lebrun, Mathias Kläui, and Martin Weides. Control of the coupling strength and linewidth of a cavity magnon-polariton. *Phys. Rev. Research*, 2:013154, Feb 2020.

[19] Yaroslav Tserkovnyak. Exceptional points in dissipatively coupled spin dynamics. *Phys. Rev. Research*, 2:013031, Jan 2020.

[20] H. Y. Yuan, Peng Yan, Shasha Zheng, Q. Y. He, Ke Xia, and Man-Hong Yung. Steady bell state generation via magnon-photon coupling. *Phys. Rev. Lett.*, 124:053602, Feb 2020.

[21] Y. Yang, Yi-Pu Wang, J. W. Rao, Y. S. Gui, B. M. Yao, W. Lu, and C.-M. Hu. Unconventional singularity in anti-parity-time symmetric cavity magnonics. *Phys. Rev. Lett.*, 125:147202, Oct 2020.

[22] Vahram L. Grigoryan and Ke Xia. Torque-induced dispersive readout in a weakly coupled hybrid system. *Phys. Rev. B*, 102:064426, Aug 2020.

[23] J.W. Rao, Y.T. Zhao, Y.S. Gui, X.L. Fan, D.S. Xue, and C.-M. Hu. Controlling microwaves in non-Hermitian metamaterials. *Phys. Rev. Applied*, 15:L021003, Feb 2021.

[24] Tian-Xiang Lu, Huilai Zhang, Qian Zhang, and Hui Jing. Exceptional-point-engineered cavity magnomechanics. *Phys. Rev. A*, 103:063708, Jun 2021.

[25] Vahram L. Grigoryan, Ka Shen, and Ke Xia. Synchronized spin-photon coupling in a microwave cavity. *Phys. Rev. B*, 98:024406, Jul 2018.

[26] Igor Proskurin, Alexander S. Ovchinnikov, Jun-ichiro Kishine, and Robert L. Stamps. Cavity optomechanics of topological spin textures in magnetic insulators. *Phys. Rev. B*, 98:220411, Dec 2018.

[27] Igor Proskurin, Rair Macêdo, and Robert L Stamps. Microscopic origin of level attraction for a coupled magnon-photon system in a microwave cavity. *New Journal of Physics*, 21(9):095003, sep 2019.

[28] Zhao-Hui Peng, Chun-Xia Jia, Yu-Qing Zhang, Ji-Bing Yuan, and Le-Man Kuang. Level attraction and $\mathcal{PT}$ symmetry in indirectly coupled microresonators. *Phys. Rev. A*, 102:043527, Oct 2020.

[29] Peng-Chao Xu, J. W. Rao, Y. S. Gui, Xiaofeng Jin, and C.-M. Hu. Cavity-mediated dissipative coupling of distant magnetic moments: Theory and experiment. *Phys. Rev. B*, 100:094415, Sep 2019.

[30] Weichao Yu, Jiongjie Wang, H. Y. Yuan, and Jiang Xiao. Prediction of attractive level crossing via a dissipative mode. *Phys. Rev. Lett.*, 123:227201, Nov 2019.

[31] J. W. Rao, Y. P. Wang, Y. Yang, T. Yu, Y. S. Gui, X. L. Fan, D. S. Xue, and C.-M. Hu. Interactions between a magnon mode and a cavity photon mode mediated by traveling photons. *Phys. Rev. B*, 101:064404, Feb 2020.

[32] Bimu Yao, Tao Yu, Xiang Zhang, Wei Lu, Yongsheng Gui, Can-Ming Hu, and Yaroslav M. Blanter. The microscopic origin of magnon-photon level attraction by traveling waves: Theory and experiment. *Phys. Rev. B*, 100:214426, Dec 2019.

[33] Jing Xu, Changchun Zhong, Xu Han, Dafei Jin, Liang Jiang, and Xufeng Zhang. Floquet cavity electromagnonics. *Phys. Rev. Lett.*, 125:237201, Dec 2020.

[34] Fabio L. Traversa, Massimiliano Di Ventra, and Fabrizio Bonani. Generalized Floquet theory: Application to dynamical systems with memory and Bloch's theorem for nonlocal potentials. *Phys. Rev. Lett.*, 110:170602, Apr 2013.

[35] Luca Magazzù, Sergey Denisov, and Peter Hänggi. Asymptotic Floquet states of non-Markovian systems. *Phys. Rev. A*, 96:042103, Oct 2017.

[36] Luca Magazzù, Sergey Denisov, and Peter Hänggi. Asymptotic Floquet states of a periodically driven spin-boson system in the nonperturbative coupling regime. *Phys. Rev. E*, 98:022111, Aug 2018.

[37] Fabio L. Traversa, Massimiliano Di Ventra, Federica Cappelluti, and Fabrizio Bonani. Application of Floquet theory to dynamical systems with memory. *Chaos*, 30(12):123102, 2020.

[38] Atsushi Ono and Sumio Ishihara. Nonequilibrium susceptibility in photoinduced Floquet states. *Phys. Rev. B*, 100:075127, Aug 2019.

[39] D. N. Zubarev, V. Morozov, and G. Röpke. *Statistical Mechanics of Nonequilibrium Processes, Vol. 2: Relaxation and Hydrodynamic Processes*. Akademie Verlag, Berlin, 1996.

[40] Naoto Tsuji, Takashi Oka, and Hideo Aoki. Correlated electron systems periodically driven out of equilibrium: Floquet + DMFT formalism. *Phys. Rev. B*, 78:235124, Dec 2008.

[41] Hideo Aoki, Naoto Tsuji, Martin Eckstein, Marcus Kollar, Takashi Oka, and Philipp Werner. Nonequilibrium dynamical mean-field theory and its applications. *Rev. Mod. Phys.*, 86:779–837, Jun 2014.

[42] Giorgio Bertotti, Claudio Serpico, and Isaak D. Mayergoyz. Nonlinear magnetization dynamics under circularly polarized field. *Phys. Rev. Lett.*, 86:724–727, Jan 2001.

[43] Morris W Hirsch, Stephen Smale, and Robert L Devaney. *Differential equations, dynamical systems, and an introduction to chaos*. Academic Press, London, 2012.

[44] Y. Li, V. V. Naletov, O. Klein, J. L. Prieto, M. Muñoz, V. Cros, P. Bortolotti, A. Anane, C. Serpico, and G. de Loubens. Nutation spectroscopy of a nanomagnet driven into deeply nonlinear ferromagnetic resonance. *Phys. Rev. X*, 9:041036, Nov 2019.

[45] Guogan Zhao, Yong Wang, and X.-F. Qian. Driven dissipative quantum dynamics in a cavity magnon-polariton system. *Phys. Rev. B*, 104:134423, Oct 2021.

[46] Alex Kamenev and Alex Levchenko. Keldysh technique and non-linear σ-model: basic principles and applications. *Advances in Physics*, 58(3):197–319, 2009.

[47] H C Fogedby. Solitons and magnons in the classical heisenberg chain. *J. Phys. A*, 13(4):1467–1499, apr 1980.

[48] I. I. Rabi, N. F. Ramsey, and J. Schwinger. Use of rotating coordinates in magnetic resonance problems. *Rev. Mod. Phys.*, 26:167–171, Apr 1954.

[49] Arne Vansteenkiste, Jonathan Leliaert, Mykola Dvornik, Mathias Helsen, Felipe Garcia-Sanchez, and Bartel Van Waeyenberge. The design and verification of mumax3. *AIP Advances*, 4(10):107133, 2014.

[50] I. G. Bostrem, E. G. Ekomasov, J. Kishine, A. S. Ovchinnikov, and V. E. Sinitsyn. Dark discrete breather modes in a monoaxial chiral helimagnet with easy-plane anisotropy. *Phys. Rev. B*, 104:214420, Dec 2021.

Chapter 4

Conclusions and future outlook

The first study reveals that DMI plays a role in modifying photon-magnon coupling and enabling coupling in a geometry where there is no coupling otherwise. This finding suggests an approach to estimate DMI parameters in antiferromagnetic materials by measuring the interaction of antiferromagnetic resonances to optical modes in a microwave cavity. This study leverages the interaction of resonances in a one-dimensional structure with optical photons and is not limited to the dynamics of a single domain wall dynamics but has potential applicability to other one-dimensional textures like chiral soliton lattice in ferromagnets and antiferromagnets. The extension of this study to two-dimensional antiferromagnetic spin textures such as skyrmions will be a problem to consider in the future.

The second study analyzed magnonics around nonlinear steady states far from equilibrium which may allow us to realize level attraction. In this description, level attraction is understood as the consequence of an instability resulting from the interaction between excitations above a stationary driven magnetization P-mode and a system of cavity photons. This work also explained the possibility of studying cavity magnonics using semi-classical dynamics by combining our theory with numerical methods to allow for cavity magnonics study using micromagnetic simulations. In this theory, all that is needed is to extract the susceptibility and one can treat arbitrary geometries that way by extracting all the dynamic information of the magnetic system from micromagnetics. This allows for future expansion. For example, the dynamics of two interacting cylindrical magnetic particles can be studied using similar techniques. The coupling between the materials will influence each other's

dynamics. They can precess in phase (low frequency) or out of phase (high frequency). This will modify how the system responds to external periodic drive. In the frequency domain, the system response is expected to show four sidebands around the driving frequency. Two side bands below and above the driving frequency will correspond to level attraction and repulsion, respectively. In both regions, the outer sidebands will correspond to the out-of-phase mode of the oscillators. The out-of-phase mode can be controlled by varying the coupling strength between the two materials. Future work will also investigate non-zero effective anisotropies and their impact on the coupling of the magnetic system to the external drive.

Appendices

Appendix A

Domain wall configuration

Our model begins with a one-dimensional (1D) Heisenberg antiferromagnetic chain, which contains even number of lattice sites. The 1D AFM chain can be described by the Hamiltonian which comprises the exchange coupling between spin vectors on two sub-lattices and uniaxial anisotropies in the $\hat{z}$ and $\hat{x}$ directions:

$$\mathcal{W} = \sum_{i=0}^{2N-1} \left[J\vec{S}_i \cdot \vec{S}_{i+1} - K_x(\vec{S}_{i,x}) - K_z(\vec{S}_{i,z}) \right], \tag{A.1}$$

We split the chain into lattice cells with sublattices A and B.

$$\mathcal{W} = \sum_{i=0}^{N-1} \left[J\left(\vec{S}_A^i \cdot \vec{S}_B^i + \vec{S}_B^i \cdot \vec{S}_A^{i+1}\right) - \frac{K_x}{2}\left((\vec{S}_A^i \cdot \hat{x})^2 + (\vec{S}_B^i \cdot \hat{x})^2\right) - \frac{K_z}{2}\left((\vec{S}_A^i \cdot \hat{z})^2 + (\vec{S}_B^i \cdot \hat{z})^2\right) \right], \tag{A.2}$$

Next, we define the total magnetization $\vec{m}_i$ and staggered magnetization, $\vec{l}_i$ of the sublattices, respectively as:

$$\vec{m}_i = \frac{\vec{S}_A^i + \vec{S}_B^i}{2S} \tag{A.3a}$$

$$\vec{l}_i = \frac{\vec{S}_A^i - \vec{S}_B^i}{2S}, \tag{A.3b}$$

subject to the constraints: $\vec{m}\cdot\vec{l}=0$ and $\vec{m}^2+\vec{l}^2=1$. From Eqs. (A.3a and A.3b),

$$\vec{S}_A^i = S(\vec{m}_i+\vec{l}_i) \tag{A.4a}$$

$$\vec{S}_B^i = S(\vec{m}_i-\vec{l}_i) \tag{A.4b}$$

By substituting Eqs. (A.4a) and (A.4b) into Eq..(A.2), the Hamiltonian reduces to a sum over the antiferromagnetic lattice points and no longer sum over spins:

$$\begin{aligned}\mathcal{W} = \sum_{i=0}^{\mathrm{N}-1}\Bigg[& JS^2\left((\vec{m}_i+\vec{l}_i)(\vec{m}_i-\vec{l}_i)+(\vec{m}_i-\vec{l}_i)(\vec{m}_{i+1}+\vec{l}_{i+1})\right)-\frac{K_xS^2}{2}\left((\vec{m}_i+\vec{l}_i)_x^2+(\vec{m}_i-\vec{l}_i)_x^2\right)\\ & -\frac{K_zS^2}{2}\left((\vec{m}_i+\vec{l}_i)_x^2+(\vec{m}_i-\vec{l}_i)_z^2\right)\Bigg]\end{aligned} \tag{A.5}$$

$$\begin{aligned}\mathcal{W} = \sum_{i=0}^{\mathrm{N}-1}\Big\{ & JS^2(\vec{m}_i-\vec{l}_i)\left[(\vec{m}_i+\vec{l}_i)+(\vec{m}_{i+1}+\vec{l}_{i+1})\right]\\ & -K_xS^2\left[(m_{i,x})^2+(l_{i,x})^2\right]-K_zS^2\left[(m_{i,z})^2+(l_{i,z})^2\right]\Big\}\end{aligned} \tag{A.6}$$

We introduce the following identities to simplify Eq. (A.6) [38]:

$$2\vec{m}_i\vec{m}_{i+1} = \vec{m}_i^2+(\vec{m}_{i+1})^2-(\vec{m}_{i+1}-\vec{m}_i)^2 \tag{A.7a}$$

$$\vec{m}_i\vec{l}_{i+1}-\vec{l}_i\vec{m}_{i+1} = \vec{m}_i(\vec{l}_{i+1}-\vec{l}_i)-\vec{l}_i(\vec{m}_{i+1}-\vec{m}_i) \tag{A.7b}$$

Substituting (A.7a) and (A.7b) into (A.6) and working through the algebra carefully, we arrive at:

$$\begin{aligned}\mathcal{W} = \sum_{i=0}^{\mathrm{N}-1}\Big\{ & JS^2\left[2(\vec{m}_i^2-\vec{l}_i^2)+\vec{m}_i(\vec{l}_{i+1}-\vec{l}_i)-\vec{l}_i(\vec{m}_{i+1}-\vec{m}_i)+\frac{1}{2}[(\vec{l}_{i+1}-\vec{l}_i)^2-(\vec{m}_{i+1}-\vec{m}_i)^2]\right]\\ & -K_xS^2(\vec{m}_{i,x}^2+\vec{l}_{i,x}^2)-K_zS^2(\vec{m}_{i,z}^2+\vec{l}_{i,z}^2)\Big\}\end{aligned} \tag{A.8}$$

We move to the continuum model:

$$\mathcal{W} = \sum_{i=0}^{\mathrm{N}-1} \Bigg\{ JS^2 \left[2(\vec{m}_i^2 - \vec{l}_i^2) + \left(\vec{m}_i \frac{\partial \vec{l}_i}{\partial z} - \vec{l}_i \frac{\partial \vec{m}_i}{\partial z} \right) a_0 + \frac{a_0^2}{2} \left(\left(\frac{\partial \vec{l}_i}{\partial z} \right)^2 - \left(\frac{\partial \vec{m}_i}{\partial z} \right)^2 \right) \right] \\ - K_x S^2 (\vec{m}_{i,x}^2 + \vec{l}_{i,x}^2) - K_z S^2 (\vec{m}_{i,z}^2 + \vec{l}_{i,z}^2) \Bigg\}, \tag{A.9}$$

where a_0 is the length of the antiferromagnetic unit cell and is equal to twice the nearest neighbour spacing in the linear chain. Converting the sums to integrals,

$$\mathcal{W} = \int_0^{L_z} \frac{dz}{a_0} \Bigg\{ 2JS^2(\vec{m}^2 - \vec{l}^2) + JS^2 a_0 \left[\vec{m} \cdot \frac{\partial \vec{l}}{\partial z} - \vec{l} \cdot \frac{\partial \vec{m}}{\partial z} \right] + JS^2 a_0^2 \left[\left(\frac{\partial \vec{l}}{\partial z} \right)^2 + \left(\frac{\partial \vec{m}}{\partial z} \right)^2 \right] \\ -K_x S^2 [(\vec{m} \cdot \hat{x})^2 + (\vec{l} \cdot \hat{x})^2] - K_z S^2 [(\vec{m} \cdot \hat{z})^2 + (\vec{l} \cdot \hat{z})^2] \Bigg\}. \tag{A.10}$$

Using the constraints, $\vec{m} \cdot \vec{l} = 0$ and $\vec{m}^2 + \vec{l}^2 = 1$, which gives: $\vec{l}^2 = 1 - \vec{m}^2$ and recognizing that $\frac{\partial}{\partial z}(\vec{m} \cdot \vec{l}) = \vec{m} \cdot \frac{\partial \vec{l}}{\partial z} + \vec{l} \cdot \frac{\partial \vec{m}}{\partial z}$ which leads to $\vec{m} \cdot \frac{\partial \vec{l}}{\partial z} = -\vec{l} \cdot \frac{\partial \vec{m}}{\partial z}$. The energy thus becomes:

$$\mathcal{W} = \int_{-\infty}^{\infty} \frac{dz}{a_0} \Bigg\{ \frac{a}{2} |\vec{m}|^2 + \frac{A}{2} \left[\left(\frac{\partial \vec{m}}{\partial z} \right)^2 + \left(\frac{\partial \vec{l}}{\partial z} \right)^2 \right] + L \left(\vec{m} \cdot \frac{\partial \vec{l}}{\partial z} \right) \\ - \frac{k_x}{2} [(\vec{m} \cdot \hat{x})^2 + (\vec{l} \cdot \hat{x})^2] - \frac{k_z}{2} [(\vec{m} \cdot \hat{z})^2 + (\vec{l} \cdot \hat{z})^2] \Bigg\}, \tag{A.11}$$

where $a = 8JS^2$ and $A = a_0^2 JS^2$ are the homogenous and non-homogenous exchange constants, respectively, $L = 2a_0 JS^2$ is the parity-breaking term [38, 24], the anisotropies are $k_z = 2K_z S^2$ and $k_x = 2K_x S^2$. We describe the dynamics of the AFM in the exchange approximation ($J \gg K$) and also consider slowly varying AFM domain wall in our description of the staggered magnetization such that $|\vec{m}|^2 \ll |\vec{l}|^2$. In this approximation, $(\partial \vec{m}/\partial z)^2 = (\vec{m}^2/\vec{l}^2)(\partial \vec{l}/\partial z)^2 \to 0$ and we neglect the anisotropic terms proportional to $(\vec{m} \cdot \hat{x})^2$ and $(\vec{m} \cdot \hat{z})^2$. We arrive at:

$$\mathcal{W} = \int_{-\infty}^{\infty} \frac{dz}{a_0} \left[\frac{a}{2} |\vec{m}|^2 + \frac{A}{2} \left| \frac{\partial \vec{l}}{\partial z} \right|^2 + L \left(\vec{m} \cdot \frac{\partial \vec{l}}{\partial z} \right) - \frac{k_x}{2} (\vec{l} \cdot \hat{x})^2 - \frac{k_z}{2} (\vec{l} \cdot \hat{z})^2 \right], \tag{A.12}$$

which when combined with the DMI terms gives Eq. (2.2) in the main text:

$$\mathcal{H}_{\rm dw} = \int_{-\infty}^{\infty} \frac{dz}{a_0} \left[\frac{a}{2}|\vec{m}|^2 + \frac{A}{2}\left|\frac{\partial \vec{l}}{\partial z}\right|^2 + L\left(\vec{m}\cdot\frac{\partial \vec{l}}{\partial z}\right) - \frac{k_z}{2}(\vec{l}\cdot\hat{z})^2 - \frac{k_x}{2}(\vec{l}\cdot\hat{x})^2 \right. \\ \left. + \vec{d}\cdot(\frac{\partial \vec{l}}{\partial z}\times\vec{l}) + \vec{d}_0\cdot(\vec{m}\times\vec{l}) \right], \tag{A.13}$$

Having obtained the Hamiltonian of the system, we proceed to derive the Lagrangian for the system by introducing the Berry phase term: $\mathcal{L}_{\rm B} = 2\hbar S\vec{m}(\partial\vec{l}/\partial t \times \vec{l})$. The Lagrangian, $\mathcal{L} = \mathcal{L}_{\rm B} - \mathcal{H}_{\rm dw}$ is:

$$\mathcal{L}_{\rm dw} = \int_{-\infty}^{\infty} \frac{dz}{a_0} \left[\rho\ \vec{m}\cdot\left(\vec{l}\times\frac{\partial \vec{l}}{\partial t}\right) - \frac{a}{2}|\vec{m}|^2 - \frac{A}{2}\left|\frac{\partial \vec{l}}{\partial z}\right|^2 - L\left(\vec{m}\cdot\frac{\partial \vec{l}}{\partial z}\right) + \frac{k_z}{2}(\vec{l}\cdot\hat{z})^2 + \frac{k_x}{2}(\vec{l}\cdot\hat{x})^2 \right. \\ \left. - \vec{d}\cdot(\frac{\partial \vec{l}}{\partial z}\times\vec{l}) - \vec{d}_0\cdot(\vec{m}\times\vec{l}) \right], \tag{A.14}$$

where $\rho = 2\hbar S$. We can exclude $\vec{m}$ from the Lagrangian by minimizing Eq. (A.14) with respect to $\vec{m}$. The result of the minimization is given in Eq. (2.3) of the main text:

$$\vec{m} = \frac{\rho}{a}\left(\vec{l}\times\frac{\partial \vec{l}}{\partial t}\right) - \frac{L}{a}\left(\frac{\partial \vec{l}}{\partial z}\right) + \frac{1}{a}\vec{d}_0\times\vec{l}, \tag{A.15}$$

Equation (2.3) implies that $\vec{m}$ is a slave variable to $\vec{l}$ [38, 24]. Substituting this result into (A.14) and simplifying, we obtain:

$$\mathcal{L}_{\rm dw} = \int_{-\infty}^{\infty} \frac{dz}{a_0} \left[\frac{\rho^2}{2a}\left(\frac{\partial \vec{l}}{\partial t}\right)^2 + \frac{3}{2a}(\vec{d}_0\times\vec{l})^2 + \frac{\rho}{a}\left(\vec{l}\times\frac{\partial \vec{l}}{\partial t}\right)\cdot(\vec{l}\times\vec{d}_0) - \frac{A}{2}\left|\frac{\partial \vec{l}}{\partial z}\right|^2 + \frac{k_z}{2}(\vec{l}\cdot\hat{z})^2 \right. \\ \left. + \frac{k_x}{2}(\vec{l}\cdot\hat{x})^2 - \vec{d}\cdot(\frac{\partial \vec{l}}{\partial z}\times\vec{l}) \right], \tag{A.16}$$

where we have neglected terms proportional to the topological term, L. We recognize that $(\vec{d}_0\times\vec{l})^2 = d_0^2 l^2 - (\vec{d}_0\cdot\vec{l})^2 = \text{constant} - (\vec{d}_0\cdot\vec{l})^2$, which will not contribute to the equations of motion. Also, we neglect the total derivatives associated with the homogenous DMI as they do not contribute to the equations of motion [24]. This leaves us with a Lagrangian which has no dependence on the total

magnetization, $\vec{m}$:

$$\mathcal{L}_{\rm dw} = \int_{-\infty}^{\infty} \frac{dz}{a_0} \left[\frac{\rho^2}{2a} \left(\frac{\partial \vec{l}}{\partial t} \right)^2 - \frac{A}{2} \left| \frac{\partial \vec{l}}{\partial z} \right|^2 + \frac{k_z}{2} (\vec{l} \cdot \hat{z})^2 + \frac{k_x}{2} (\vec{l} \cdot \hat{x})^2 - \vec{d} \cdot \left(\frac{\partial \vec{l}}{\partial z} \times \vec{l} \right) \right] . \tag{A.17}$$

For the static configuration, we set $\partial \vec{l}/\partial t = 0$ and parametrize $\vec{l}$ by polar and azimuthal angles in spherical coordinates: $\vec{l} = (\sin\theta\cos\phi, \sin\theta\sin\phi, \cos\theta)$. The equivalent Hamiltonian of the system given by Eq. (2.5) in the main text is:

$$\mathcal{H}_{\rm dw} = \int_{-\infty}^{\infty} \frac{dz}{a_0} \left[A \left(\frac{\partial \theta}{\partial z} \right)^2 - k_x \sin^2\theta \cos^2\phi - k_z \cos^2\theta - d_x \left(\frac{\partial \theta}{\partial z} \right) \sin\phi + d_y \left(\frac{\partial \theta}{\partial z} \right) \cos\phi \right] , \tag{A.18}$$

Appendix B

Dzyalonshinskii-Moriya interaction (DMI)

The DMI between two atomic spins S_i and S_{i+1} can be expressed as vector product formed by the magnetic moments S_i of two magnetic ions,

$$\mathcal{H}_{\mathrm{DMI}} = \sum_i (-1)^i \vec{D} \cdot (\vec{S}_i \times \vec{S}_{i+1}) \tag{B.1}$$

When written in terms of the nearest neighbouring spins on the sublattices, we have

$$\mathcal{H}_{\mathrm{DMI}} = \sum_n \vec{D} \cdot (\vec{S}_n^A \times \vec{S}_n^B) + \vec{D}(\vec{S}_{n+1}^A \times \vec{S}_n^B)$$

where $\vec{S}^A = \vec{m} + \vec{l}$ and $\vec{S}^B = \vec{m} - \vec{l}$. Substituting these into the previous expression and doing some lines of vector algebra, we arrive at the expression:

$$\begin{aligned} \mathcal{H}_{\mathrm{DMI}} = \sum_n \Big\{ & 4\vec{D}S^2 \cdot (\vec{m}_n \times \vec{l}_n) - \vec{D}S^2 [\vec{m}_{n+1} \times \vec{m}_n - \vec{l}_{n+1} \times \vec{l}_n - (\vec{m}_{n+1} - \vec{m}_n) \times \vec{l}_n \\ & + (\vec{l}_{n+1} - \vec{l}_n) \times \vec{m}_n] \Big\} \end{aligned} \tag{B.2}$$

In the continuum limit,

$$\mathcal{H}_{\text{DMI}} = \int \frac{dz}{a_0} \left\{ \vec{d}_0 \cdot (\vec{m} \times \vec{l}) - \left[\vec{d} \cdot \left(\frac{\partial \vec{m}}{\partial z} \times \vec{m} \right) - \vec{d} \cdot \left(\frac{\partial \vec{l}}{\partial z} \times \vec{l} \right) - \vec{d} \cdot \left(\frac{\partial \vec{m}}{\partial z} \times \vec{l} \right) + \vec{d} \cdot \left(\frac{\partial \vec{l}}{\partial z} \times \vec{m} \right) \right] \right., \tag{B.3}$$

where $\vec{d}_0 = 4S^2\vec{D}$ and $\vec{d} = a_0 S^2 \vec{D}$. Integrating by parts, we find that $\vec{d} \cdot \left(\frac{\partial \vec{m}}{\partial z} \times \vec{l} \right) = \vec{d} \cdot \left(\frac{\partial \vec{l}}{\partial z} \times \vec{m} \right)$ and thus the last two terms cancel out. Neglecting the second term, we are arrive at:

$$\mathcal{H}_{\text{DMI}} = \int \frac{dz}{a_0} \left\{ \vec{d}_0 \cdot (\vec{m} \times \vec{l}) + \vec{d} \cdot \left(\frac{\partial \vec{l}}{\partial z} \times \vec{l} \right) \right\} \tag{B.4}$$

The Lagrangian of the system which includes the DMI term in Eq. (B.4) is varied with respect to $\vec{m}$ to obtain an expression for $\vec{m}$ as a slave variable to $\vec{l}$ which depends on $\vec{d}_0$, $\vec{l}$, and the spatial and temporal derivatives of $\vec{l}$:

$$\vec{m} = \frac{\rho}{a} \left(\vec{l} \times \frac{\partial \vec{l}}{\partial t} \right) - \frac{L}{a} \left(\frac{\partial \vec{l}}{\partial z} \right) + \frac{1}{a} \vec{d}_0 \times \vec{l}, \tag{B.5}$$

where a is the homogeneous exchange constant.

DMI-dependent equations of motion

The equations of motion in the presence of DMI are given. First, we consider the case where electromagnetic waves propagating along $\hat{x}$ couple to the wall position with DMI present in the $\hat{y}$ direction. The equations of motion in frequency space

$$\begin{pmatrix} -i(\omega - \Omega_m) & 0 & -gy_1 & -gy_1 \\ 0 & -i(\omega + \Omega_m) & -gy_2 & -gy_2 \\ gy_2 & -gy_1 & -i(\omega - \Delta) & 0 \\ -gy_2 & gy_1 & 0 & -i(\omega + \Delta) \end{pmatrix} \begin{pmatrix} \delta\hat{b} \\ \delta\hat{b}^\dagger \\ \delta\hat{a} \\ \delta\hat{a}^\dagger \end{pmatrix} = \begin{pmatrix} 0 \\ 0 \\ -i\varepsilon \\ i\varepsilon* \end{pmatrix}, \tag{B.6}$$

where $y_1 = (\pi\Omega_m \sin\phi - 2id_y)$, $y_2 = (\pi\Omega_m \sin\phi + 2id_y)$. In this configuration, the propagating wave is in the hard axis of the wall and results in no magneto-optical coupling. We found that for DMI to play a role, it must be perpendicular to both the wall direction ($\hat{z}$) and the direction of propagating wave

($\hat{x}$). Therefore, we consider DMI present along $\hat{y}$. The presence of DMI breaks the degeneracy which occurs at resonance and allows for magneto-optical coupling which depends on the y-component of the DMI vector.

The second geometry considered is the one in which electromagnetic wave propagating along $\hat{y}$ couples to the wall position with DMI present in the $\hat{x}$ direction. The electromagnetic wave is circularly polarized in the easy plane of the domain wall. As a result, there is a strong coupling. The plot of hybridized frequency against the detuning parameter is shown in Fig (2.3b). We draw the conclusion that in this geometry whether DMI is present or not, there is coupling of photons to magnons, however the presence of DMI leads to modulation of the frequencies. The equation of motion is given in matrix form:

$$\begin{pmatrix} -i(\omega-\Omega_m) & 0 & gx_1 & gx_1 \\ 0 & -i(\omega+\Omega_m) & gx_2 & gx_2 \\ -gx_2 & gx_1 & -i(\omega-\Delta) & 0 \\ gx_2 & -gx_1 & 0 & -i(\omega+\Delta) \end{pmatrix} \begin{pmatrix} \delta\hat{b} \\ \delta\hat{b}^\dagger \\ \delta\hat{a} \\ \delta\hat{a}^\dagger \end{pmatrix} = \begin{pmatrix} 0 \\ 0 \\ -i\varepsilon \\ i\varepsilon* \end{pmatrix}, \tag{B.7}$$

where $x_1 = (\pi\Omega_m \cos\phi - 2id_x)$ and $x_2 = (\pi\Omega_m \cos\phi + 2id_x)$.

Appendix C

Master equation for open systems

By applying Tr_r to both sides of Eq. (3.2), we obtain (note that the source term disappears under this transformation)

$$\left(\frac{\partial}{\partial t} + i\mathcal{L}_s^t\right)\hat{\rho}(t) = -\,\mathrm{Tr}_r\left(i\mathcal{L}_i^t\hat{\rho}_{\mathrm{tot}}(t)\right). \tag{C.1}$$

To close this equation, we introduce $\Delta\hat{\rho}(t)$ using the following definition

$$\hat{\rho}_{\mathrm{tot}}(t) = \hat{\rho}(t)\hat{\rho}_r(t) + \Delta\hat{\rho}(t), \tag{C.2}$$

with the boundary condition $\Delta\hat{\rho}(t) = 0$ at $t \to -\infty$. From Eqs. (3.2) and (C.1), after a little algebra, we find that

$$\left(\frac{\partial}{\partial t} + i\mathcal{L}_s^t + i\mathcal{L}_r^t + i\mathcal{L}_i^t + \varepsilon\right)\Delta\hat{\rho}(t) = -i\mathcal{L}_i^t\hat{\rho}(t)\hat{\rho}_r(t) + \mathrm{Tr}_r\left[i\mathcal{L}_i^t\hat{\rho}_{\mathrm{tot}}(t)\right]\hat{\rho}_r(t) - \hat{\rho}(t)\left(\frac{\partial\hat{\rho}_r(t)}{\partial t} + i\mathcal{L}_r^t\hat{\rho}_r(t)\right). \tag{C.3}$$

The last term on the right hand side vanishes, since $\hat{\rho}_r(t)$ satisfies Eq. (3.3). This equation contains $\Delta\hat{\rho}(t)$ in the second term at the right hand side.

To deal with the second term, we introduce a projection operator

$$\mathcal{P}_t\,\hat{A} = \hat{\rho}_r(t)\,\mathrm{Tr}_r\,\hat{A}, \tag{C.4}$$

where $\hat{A}$ is any operator in the Hilbert space of the whole system. Note that since we consider the reservoir to be dynamics, $\mathcal{P}_t$ can bring additional time dependence. With the help of this definition,

we find

$$\mathrm{Tr}_r\left(i\mathcal{L}_i^t\hat{\rho}_{\mathrm{tot}}(t)\right)\hat{\rho}_r(t) = \mathcal{P}_t\, i\mathcal{L}_i^t\hat{\rho}_{\mathrm{tot}}(t) = \mathcal{P}_t\, i\mathcal{L}_i^t\hat{\rho}(t)\hat{\rho}_r(t) + \mathcal{P}_t\, i\mathcal{L}_i^t\Delta\hat{\rho}(t). \tag{C.5}$$

This allows to rewrite Eq. (C.3) in the following form

$$\left(\frac{\partial}{\partial t} + i\mathcal{L}_s^t + i\mathcal{L}_r^t + \mathcal{Q}_t\, i\mathcal{L}_i^t\, \mathcal{Q}_t + \varepsilon\right)\Delta\hat{\rho}(t) = -i\mathcal{L}_i^t\hat{\rho}(t)\hat{\rho}_r(t) + \mathcal{P}_t\, i\mathcal{L}_i^t\hat{\rho}(t)\hat{\rho}_r(t), \tag{C.6}$$

where $\mathcal{Q}_t = 1 - \mathcal{P}_t$.

Finally, the right hand side of this equation can be simplified using the following identity

$$\mathrm{Tr}_r\, i\mathcal{L}_i^t\hat{\rho}(t)\hat{\rho}_r(t) = \frac{1}{i\hbar}\left[\hat{\rho}(t), \mathrm{Tr}_r\left(\hat{H}_i^t\hat{\rho}_r(t)\right)\right], \tag{C.7}$$

which gives

$$\left(\frac{\partial}{\partial t} + i\mathcal{L}_s^t + i\mathcal{L}_r^t + \mathcal{Q}_t\, i\mathcal{L}_i^t\, \mathcal{Q}_t + \varepsilon\right)\Delta\hat{\rho}(t) = -i\Delta\mathcal{L}_i^t\hat{\rho}(t)\hat{\rho}_r(t). \tag{C.8}$$

where the Liouville operator at the right hand side is defined as follows

$$i\Delta\mathcal{L}_i^t\ldots = \frac{1}{i\hbar}\left[\ldots, \Delta\hat{H}_i^t\right], \quad \text{where} \quad \Delta\hat{H}_i^t = \hat{H}_i^t - \mathrm{Tr}_r\left(\hat{H}_i^t\hat{\rho}_r(t)\right). \tag{C.9}$$

C.1 Formal solution for $\Delta\hat{\rho}(t)$ and master equation for $\hat{\rho}(t)$

Formal solution of the Liouville equation (C.8) is

$$\Delta\hat{\rho}(t) = -\int_{-\infty}^{t} dt' \mathcal{U}_{tt'} i\Delta\mathcal{L}_i^{t'}\hat{\rho}(t')\hat{\rho}_r(t'), \tag{C.10}$$

and the evolution operator is given by

$$\mathcal{U}_{tt'} = \mathcal{T}\exp\left[-\int_{t'}^{t} d\tau\left(i\mathcal{L}_s^\tau + i\mathcal{L}_r^\tau + \mathcal{Q}_\tau i\mathcal{L}_i^\tau\mathcal{Q}_\tau + \varepsilon\right)\right], \qquad t > t', \tag{C.11}$$

where $\mathcal{T}$ is the time ordering operator.

This allows us to write down an equation for $\hat{\rho}(t)$ in a closed form

$$\left(\frac{\partial}{\partial t}+i\mathcal{L}_s^t\right)\hat{\rho}(t)+\mathrm{Tr}_r\left[i\mathcal{L}_i^t\hat{\rho}(t)\hat{\rho}_r(t)\right]$$
$$=\int_{-\infty}^{t}dt'e^{-\varepsilon(t-t')}\,\mathrm{Tr}_r\,i\mathcal{L}_i^t\mathcal{T}\exp\left\{-\int_{t'}^{t}d\tau\left(i\mathcal{L}_s^\tau+i\mathcal{L}_r^\tau+\mathcal{Q}_\tau i\mathcal{L}_i^\tau\mathcal{Q}_\tau\right)\right\}i\Delta\mathcal{L}_i^{t'}\hat{\rho}(t')\hat{\rho}_r(t'). \quad \text{(C.12)}$$

The fact that $\mathrm{Tr}_r\left(\Delta\hat{\rho}(t)\right)=0$ allows us to replace $i\mathcal{L}_i^t$ with $i\Delta\mathcal{L}_i^t$ in this equation, so that it would have a symmetric form.

In the weak interaction limit, a great simplification is achieved by neglecting the higher order interaction terms, $\mathcal{Q}_\tau i\mathcal{L}_i^\tau\mathcal{Q}_\tau$, inside the argument of the exponent at the right hand side of Eq. (C.12), which also disentangles evolution operators for the probe system and reservoir. In this approximation, the right hand side is of the second order in $\hat{H}_i^t$.

Now, by transforming the Liouville operators into the commutators, we can rewrite the master equation for $\hat{\rho}(t)$ the following form

$$\frac{\partial\hat{\rho}(t)}{\partial t}+\frac{1}{i\hbar}\left[\hat{\rho}(t),\hat{H}_s^t+\mathrm{Tr}_r\left(\hat{H}_i^t\hat{\rho}_r(t)\right)\right]=\frac{1}{(i\hbar)^2}\int_{-\infty}^{t}dt'e^{-\varepsilon(t-t')}\,\mathrm{Tr}_r\left[\hat{H}_i^t,\hat{U}_{tt'}\left[\Delta\hat{H}_i^{t'},\hat{\rho}(t')\hat{\rho}_r(t')\right]\hat{U}_{tt'}^{-1}\right], \quad \text{(C.13)}$$

where the evolution operator is defined in Eq. (3.5).

The next simplification is reached by observing that dynamics of $\hat{\rho}_r(t)$ is independent from dynamics of the probe, and satisfies equation (3.3), so that $\hat{U}_{tt'}\hat{\rho}_r(t')\hat{U}_{tt'}^{-1}=\hat{\rho}_r(t)$.

By introducing shorthand notations $\hat{\rho}(t,t')=\hat{U}_{tt'}\hat{\rho}(t')\hat{U}_{tt'}^{-1}$ and $\Delta\hat{H}_i^{t'}(t,t')=\hat{U}_{tt'}\Delta\hat{H}_i^{t'}\hat{U}_{tt'}^{-1}$, we rewrite the master equation for $\hat{\rho}(t)$ in the weak interaction limit in the form of Eq. (3.4).

C.2 Kinetic equations for dynamic variables

Further simplification is reached by considering the interaction Hamiltonian in the following form $\hat{H}_i=\hat{A}\hat{F}+\hat{A}^\dagger\hat{F}^\dagger$, where the operators $\hat{A}$ and $\hat{A}^\dagger$ act in the Hilbert space of the probe system and $\hat{F}$ and $\hat{F}^\dagger$ act entirely on the degrees of freedom of the reservoir. In this case, $\Delta\hat{H}_i^{t'}=\hat{A}\Delta\hat{F}_{t'}+\hat{A}^\dagger\Delta\hat{F}_{t'}^\dagger$, where $\Delta\hat{F}_{t'}=\hat{F}-\langle\hat{F}\rangle_r^{t'}$, and $\langle\hat{F}\rangle_r^{t'}=\mathrm{Tr}_r\left[\hat{F}\hat{\rho}_r(t')\right]$. We do not specify any specific commutation rules for $\hat{A}$ and $\hat{A}^\dagger$ at this stage.

The explicit form of the master equation for $\hat{\rho}(t)$ is obtained straightforwardly from Eq. (3.4)

$$\frac{\partial\hat{\rho}(t)}{\partial t}+\frac{1}{i\hbar}\left[\hat{\rho}(t),\hat{H}_s^t\right]+\frac{1}{i\hbar}\left[\hat{\rho}(t),\hat{A}\right]\langle\hat{F}\rangle_r^t+\frac{1}{i\hbar}\left[\hat{\rho}(t),\hat{A}^\dagger\right]\langle\hat{F}^\dagger\rangle_r^t=\frac{1}{(i\hbar)^2}\int_{-\infty}^{t}dt'e^{-\varepsilon(t-t')}$$
$$\times\Big\{\langle\hat{F}\Delta\hat{F}_{t'}(t,t')\rangle_r^t\hat{A}\hat{A}(t,t')\hat{\rho}(t,t')+\langle\hat{F}^\dagger\Delta\hat{F}_{t'}^\dagger(t,t')\rangle_r^t\hat{A}^\dagger\hat{A}^\dagger(t,t')\hat{\rho}(t,t')+\langle\hat{F}\Delta\hat{F}_{t'}^\dagger(t,t')\rangle_r^t\hat{A}\hat{A}^\dagger(t,t')\hat{\rho}(t,t')$$
$$+\langle\hat{F}^\dagger\Delta\hat{F}_{t'}(t,t')\rangle_r^t\hat{A}^\dagger\hat{A}(t,t')\hat{\rho}(t,t')+\langle\Delta\hat{F}_{t'}(t,t')\hat{F}\rangle_r^t\hat{\rho}(t,t')\hat{A}(t,t')\hat{A}+\langle\Delta\hat{F}_{t'}^\dagger(t,t')\hat{F}^\dagger\rangle_r^t\hat{\rho}(t,t')\hat{A}^\dagger(t,t')\hat{A}^\dagger$$
$$+\langle\Delta\hat{F}_{t'}(t,t')\hat{F}^\dagger\rangle_r^t\hat{\rho}(t,t')\hat{A}(t,t')\hat{A}^\dagger+\langle\Delta\hat{F}_{t'}^\dagger(t,t')\hat{F}\rangle_r^t\hat{\rho}(t,t')\hat{A}^\dagger(t,t')\hat{A}-\langle\Delta\hat{F}_{t'}(t,t')\hat{F}\rangle_r^t\hat{A}\hat{\rho}(t,t')\hat{A}(t,t')$$
$$-\langle\Delta\hat{F}_{t'}^\dagger(t,t')\hat{F}^\dagger\rangle_r^t\hat{A}^\dagger\hat{\rho}(t,t')\hat{A}^\dagger(t,t')-\langle\Delta\hat{F}_{t'}^\dagger(t,t')\hat{F}\rangle_r^t\hat{A}\hat{\rho}(t,t')\hat{A}^\dagger(t,t')-\langle\Delta\hat{F}_{t'}(t,t')\hat{F}^\dagger\rangle_r^t\hat{A}^\dagger\hat{\rho}(t,t')\hat{A}(t,t')$$
$$-\langle\hat{F}\Delta\hat{F}_{t'}(t,t')\rangle_r^t\hat{A}(t,t')\hat{\rho}(t,t')\hat{A}-\langle\hat{F}^\dagger\Delta\hat{F}_{t'}^\dagger(t,t')\rangle_r^t\hat{A}^\dagger(t,t')\hat{\rho}(t,t')\hat{A}^\dagger-\langle\hat{F}^\dagger\Delta\hat{F}_{t'}(t,t')\rangle_r^t\hat{A}(t,t')\hat{\rho}(t,t')\hat{A}^\dagger$$
$$-\langle\hat{F}\Delta\hat{F}_{t'}^\dagger(t,t')\rangle_r^t\hat{A}^\dagger(t,t')\hat{\rho}(t,t')\hat{A}\Big\}\quad\text{(C.14)}$$

where we used shorthand notations $\hat{A}(t,t')=\hat{U}_{tt'}\hat{A}\hat{U}_{tt'}^{-1}$ and $\hat{F}(t,t')=\hat{U}_{tt'}\hat{F}\hat{U}_{tt'}^{-1}$, and $\langle\ldots\rangle_r^t\equiv\mathrm{Tr}_r[\ldots\hat{\rho}_r(t)]$.

Correlation functions between $\hat{F}$ and $\hat{F}^\dagger$ in this equations can be transformed to a more physically transparent form. For this purpose, we introduce the Heisenberg picture for operators as follows

$$\hat{A}(t)=\hat{U}_{t,-\infty}^{-1}\hat{A}\hat{U}_{t,-\infty},\quad\text{(C.15)}$$

where the explicit expressions for the evolution operators are given by

$$\hat{U}_{t,-\infty}=\mathcal{T}\exp\left(-\frac{i}{\hbar}\int_{-\infty}^{t}\hat{H}_r^\tau d\tau\right)\quad\text{and}\quad\hat{U}_{t,-\infty}^{-1}=\mathcal{T}_a\exp\left(\frac{i}{\hbar}\int_{-\infty}^{t}\hat{H}_r^\tau d\tau\right).\quad\text{(C.16)}$$

In this notation, we can express these correlation functions in terms of nonequilibrium Green functions [39]

$$\langle\hat{F}^\dagger\hat{F}(t,t')\rangle_r^t=\langle\hat{F}^\dagger(t)\hat{F}(t')\rangle_r\equiv\mathrm{Tr}_r\left\{\hat{F}^\dagger(t)\hat{F}(t')\rho_r(-\infty)\right\},\quad t>t'.\quad\text{(C.17)}$$

We now apply the master equation for $\hat{\rho}(t)$ to derive kinetic equations for dynamic variables. For a dynamics variable described by a general operator $\hat{B}$ in the Hilbert space of the probe system, we define the average value at time moment t as $\langle\hat{B}\rangle^t=\mathrm{Tr}\left[\hat{B}\hat{\rho}(t)\right]$. In this case using Eq. (C.14), we

find

$$\frac{d}{dt}\langle\hat{B}\rangle^t+\frac{1}{i\hbar}\left\langle\left[\hat{H}_s^t,\hat{B}\right]\right\rangle^t+\frac{1}{i\hbar}\langle\hat{F}^\dagger\rangle_r^t\left\langle\left[\hat{A}^\dagger,\hat{B}\right]\right\rangle^t+\frac{1}{i\hbar}\langle\hat{F}\rangle_r^t\left\langle\left[\hat{A},\hat{B}\right]\right\rangle^t=\frac{1}{(i\hbar)^2}\int_{-\infty}^{t}dt'e^{-\varepsilon(t-t')}$$
$$\times\Big\{\langle\hat{F}\Delta\hat{F}_{t'}(t,t')\rangle_r^t\langle[\hat{B}(t',t),\hat{A}(t',t)]\hat{A}\rangle^{t'}+\langle\hat{F}^\dagger\Delta\hat{F}_{t'}^\dagger(t,t')\rangle_r^t\langle[\hat{B}(t',t),\hat{A}^\dagger(t',t)]\hat{A}^\dagger\rangle^{t'}$$
$$+\langle\hat{F}\Delta\hat{F}_{t'}^\dagger(t,t')\rangle_r^t\langle[\hat{B}(t',t),\hat{A}(t',t)]\hat{A}^\dagger\rangle^{t'}+\langle\hat{F}^\dagger\Delta\hat{F}_{t'}(t,t')\rangle_r^t\langle[\hat{B}(t',t),\hat{A}^\dagger(t',t)]\hat{A}\rangle^{t'}$$
$$+\langle\Delta\hat{F}_{t'}(t,t')\hat{F}\rangle_r^t\langle\hat{A}[\hat{A}(t',t),\hat{B}(t',t)]\rangle^{t'}+\langle\Delta\hat{F}_{t'}^\dagger(t,t')\hat{F}\rangle_r^t\langle\hat{A}^\dagger[\hat{A}^\dagger(t',t),\hat{B}(t',t)]\rangle^{t'}$$
$$+\langle\Delta\hat{F}_{t'}(t,t')\hat{F}^\dagger\rangle_r^t\langle\hat{A}[\hat{A}^\dagger(t',t),\hat{B}(t',t)]\rangle^{t'}+\langle\Delta\hat{F}_{t'}^\dagger(t,t')\hat{F}\rangle_r^t\langle\hat{A}^\dagger[\hat{A}(t',t),\hat{B}(t',t)]\rangle^{t'}\Big\},\quad(C.18)$$

where $\hat{B}(t',t)=\hat{U}_{tt'}^{-1}\hat{B}\hat{U}_{tt'}$.

In what follows, we will be interested in a situation when $\hat{B}$ is the same dynamic variable as in $\hat{H}_i$, i. e. $\hat{B}=\hat{A}$. In this case, the kinetic equation is simplified

$$\frac{d}{dt}\langle\hat{A}\rangle^t+\frac{1}{i\hbar}\left\langle\left[\hat{H}_s^t,\hat{A}\right]\right\rangle^t+\frac{1}{i\hbar}\langle\hat{F}^\dagger\rangle_r^t\left\langle\left[\hat{A}^\dagger,\hat{A}\right]\right\rangle^t=\frac{1}{(i\hbar)^2}\int_{-\infty}^{t}dt'e^{-\varepsilon(t-t')}$$
$$\times\Big\{\langle\hat{F}^\dagger\Delta\hat{F}_{t'}^\dagger(t,t')\rangle_r^t\langle[\hat{A}(t',t),\hat{A}^\dagger(t',t)]\hat{A}^\dagger\rangle^{t'}+\langle\hat{F}^\dagger\Delta\hat{F}_{t'}(t,t')\rangle_r^t\langle[\hat{A}(t',t),\hat{A}^\dagger(t',t)]\hat{A}\rangle^{t'}$$
$$+\langle\Delta\hat{F}_{t'}^\dagger(t,t')\hat{F}^\dagger\rangle_r^t\langle\hat{A}^\dagger[\hat{A}^\dagger(t',t),\hat{A}(t',t)]\rangle^{t'}+\langle\Delta\hat{F}_{t'}(t,t')\hat{F}^\dagger\rangle_r^t\langle\hat{A}[\hat{A}^\dagger(t',t),\hat{A}(t',t)]\rangle^{t'}\Big\}.\quad(C.19)$$

And finally, if $\hat{A}=\hat{a}$, where $\hat{a}$ and $\hat{a}^\dagger$ satisfy the boson commutation rules, $[\hat{a},\hat{a}^\dagger]=1$, and we obtain

$$\frac{d\langle\hat{a}\rangle^t}{dt}+\frac{1}{i\hbar}\left\langle\left[\hat{H}_s^t,\hat{a}\right]\right\rangle^t-\frac{1}{i\hbar}\langle\hat{F}^\dagger\rangle_r^t=\frac{1}{(i\hbar)^2}\int_{-\infty}^{t}dt'e^{-\varepsilon(t-t')}\Big\{\langle[\hat{F}^\dagger,\hat{F}^\dagger(t,t')]\rangle_r^t\langle\hat{a}^\dagger\rangle^{t'}+\langle[\hat{F}^\dagger,\hat{F}(t,t')]\rangle_r^t\langle\hat{a}\rangle^{t'}\Big\}.$$

A contribution from the off-resonant term, proportional to $\langle[\hat{F}^\dagger(t),\hat{F}^\dagger(t')]\rangle_r$, is usually small compared to $\langle[\hat{F}^\dagger(t),\hat{F}(t')]\rangle_r$, which describes resonant interaction between the probe system and reservoir. If ω_0 is a characteristic frequency of the reservoir, the off-resonant term oscillates at $2\omega_0$, and can be neglected when $\omega\tau_r\gg1$, where τ_r is a characteristic relaxation time of the reservoir [39].

If we neglect the off-resonant term proportional to $\langle\hat{a}^\dagger\rangle^t$ and use the identity in Eq. (C.17), we obtain the following kinetic equation for $\langle\hat{a}\rangle^t$

$$i\hbar\frac{d\langle\hat{a}\rangle^t}{dt}+\left\langle\left[\hat{H}_s^t,\hat{a}\right]\right\rangle^t-\int_{-\infty}^{t}dt'G(t,t')\langle\hat{a}\rangle^{t'}=\langle\hat{F}^\dagger\rangle_r^t,\quad(C.20)$$

where we introduce nonequilibrium retarded Green function

$$G(t,t') = \frac{e^{-\varepsilon(t-t')}}{i\hbar}\theta(t-t')\langle[\hat{F}^\dagger(t),\hat{F}(t')]\rangle_r, \tag{C.21}$$

where the operators $\hat{F}$ and $\hat{F}^\dagger$ are in the Heisenberg picture as defined by Eq (C.15), and $\langle\ldots\rangle_r \equiv \mathrm{Tr}_r\left(\ldots\hat{\rho}_r(-\infty)\right)$.

Appendix D

Perturbative expansion over a P-mode solution

Here, we discuss how to calculate spin-spin Poisson brackets for linear excitations around a stationary **P**-mode trajectory. The Poisson bracket for two circularly polarized spin components $S^{(\pm)}$ taken at different time moments is defined in Eq. (3.10). For this purpose, we expand the equations of motion (3.13) and (3.14) over the stationary **P**-mode solution: $\theta(t) = \theta_0 + \delta\theta(t)$ and $\phi(t) = \phi_0 + \delta\phi(t)$, where θ_0 and ϕ_0 denote stationary solution defined in Eq. (3.15) and (3.16). To linear order in $\delta\phi(t)$ and $\delta\theta(t)$, the equations of motion become

$$\delta\dot{\theta} - \alpha \sin\theta_0 \delta\dot{\phi} = \varkappa \left(b_\perp \cos\phi_0 \delta\phi - \Omega \cos\theta_0 \delta\theta\right), \tag{D.1}$$

$$\alpha\delta\dot{\theta} + \sin\theta_0 \delta\dot{\phi} = -\varkappa \left(b_\perp \sin\phi_0 \cos\theta_0 \delta\phi + b_\perp \cos\phi_0 \sin\theta_0 \delta\theta + b_z \cos\theta_0 \delta\theta + \cos 2\theta_0 \delta\theta\right). \tag{D.2}$$

These equations are also given in the matrix form in Eq. (3.17). Two important characteristics of this equation are the trace and the determinant of the matrix on the right hand side of Eq. (3.17) (denoted here as M):

$$\mathrm{Tr}\, M = -\frac{2\alpha\varkappa}{1+\alpha^2}\left(v - \frac{1-m_z^2}{2} + \frac{\Omega m_z}{\alpha}\right), \quad \det M = \frac{\varkappa^2}{1+\alpha^2}\left(v^2 - (1-m_z^2)v + \Omega^2 m_z^2\right), \tag{D.3}$$

from which a phase diagram for **P**-mode stability can be obtained [42].

Let us first illustrate how to calculate this Poisson bracket in absence of anisotropy, $\varkappa = 0$, and

dissipation, $\alpha = 0$. In this case, the equations of motion in (D.1) and (D.2) reduce for those of a harmonic oscillator

$$\delta\dot{\theta} = h_{a\perp}\delta\phi, \qquad \delta\dot{\phi} = -\frac{h_{a\perp}}{\sin^2\theta_0}\delta\theta. \tag{D.4}$$

Solutions for these equation, which satisfies the initial conditions $\delta\phi(0) = \delta\phi_0$ and $\delta\theta(0) = \delta\theta_0$, have the following form

$$\delta\theta(t) = \delta\theta_0 \cos\omega_0 t + \frac{h_{a\perp}}{\tilde{\omega}_0}\delta\phi_0 \sin\omega_0 t, \tag{D.5}$$

$$\delta\phi(t) = -\frac{\tilde{\omega}_0}{h_{a\perp}}\delta\theta_0 \sin\omega_0 t + \delta\phi_0 \cos\omega_0 t, \tag{D.6}$$

where $\tilde{\omega}_0 = h_{a\perp}/\sin\theta_0$ denotes the dimensionless frequency.

In this situation, $S^{(+)}(t)$ is expanded around the **P**-mode as follows

$$S^{(+)}(t) = \sin\theta_0 e^{i\omega' t} + e^{i(\omega'+\omega_0)t}\cos^2\frac{\theta_0}{2}\left(\delta\theta_0 - i\sin\theta_0\delta\phi_0\right) - e^{i(\omega'-\omega_0)t}\sin^2\frac{\theta_0}{2}\left(\delta\theta_0 + i\sin\theta_0\delta\phi_0\right). \tag{D.7}$$

From the definition of the Poisson bracket in Eq. (3.10), we restore Eq. (3.18) in the main text. Note that in the limit of $\theta_0 \to 0$, this expression reduces to $\{S^{(+)}(t), S^{(-)}(0)\} \to -2ie^{i(\omega'+\omega_0)t}$, where $\omega_0 \approx \gamma B_z - \omega'$, which corresponds to the usual ferromagnetic resonance with the frequency γB_z.

The explicit expression for the spin-spin Poisson bracket in the general case is given by

$$\{S^{(+)}(t), S^{(-)}(0)\} = \frac{e^{i\omega' t}}{\sin\theta_0}\left[\cos^2\theta_0\frac{\partial\delta\theta(t)}{\partial\delta\phi_0} - \sin^2\theta_0\frac{\partial\delta\phi(t)}{\partial\delta\theta_0} - i\sin\theta_0\cos\theta_0\left(\frac{\partial\delta\phi(t)}{\partial\delta\phi_0} + \frac{\partial\delta\theta(t)}{\partial\delta\theta_0}\right)\right], \tag{D.8}$$

where $\delta\phi(t)$ and $\delta\theta(t)$ satisfy Eq. (3.17) with $\delta\theta(0) = \delta\theta_0$ and $\delta\phi(0) = \delta\phi_0$. A solution of Eq. (3.17) that satisfy these initial conditions can be written in the following general form

$$\begin{pmatrix}\delta\theta(t)\\ \delta\phi(t)\end{pmatrix} = e^{-\gamma t}\left[\frac{\delta\theta_0 v_2 - \delta\phi_0 v_1}{u_1 v_2 - u_2 v_1}\begin{pmatrix}u_1\\ u_2\end{pmatrix}e^{i\omega_0 t} + \frac{\delta\phi_0 u_1 - \delta\theta_0 u_2}{u_1 v_2 - u_2 v_1}\begin{pmatrix}v_1\\ v_2\end{pmatrix}e^{-i\omega_0 t}\right], \tag{D.9}$$

where $(u_1, u_2)^T$ is the eigenvector (not necessary normalized) that corresponds to $\lambda_+ = -\gamma + i\omega_0$ and $(v_1, v_2)^T$ corresponds to $\lambda_- = -\gamma - i\omega_0$. The explicit expressions (in dimensionless units) can be

found from Eq. (3.17) and (D.3)

$$\tilde{\lambda}_{\pm} = \frac{1}{2}\left(\operatorname{tr} M \pm \sqrt{(\operatorname{tr} M)^2 - 4\det M}\right) \equiv -\tilde{\gamma} \pm i\tilde{\omega}_0, \tag{D.10}$$

where $\tilde{\gamma} = -\frac{1}{2}\operatorname{tr} M$, and $i\tilde{\omega}_0 = \sqrt{(\operatorname{tr} M)^2 - 4\det M}$. For components of the eigenvectors we have

$$\begin{pmatrix} u_1 & v_1 \\ u_2 & v_2 \end{pmatrix} = \begin{pmatrix} -\dfrac{\sin\theta_0(v - \alpha\Omega m_z)}{\frac{1}{2}\alpha(1-m_z^2) - i\tilde{\omega}_0} & -\dfrac{\sin\theta_0(v - \alpha\Omega m_z)}{\frac{1}{2}\alpha(1-m_z^2) + i\tilde{\omega}_0} \\ 1 & 1 \end{pmatrix}. \tag{D.11}$$

By expanding $S^{(+)}(t)$ around the stationary solution and calculating the derivatives with respect to the initial condition in Eq. (D.8), we obtain

$$\{S^{(+)}(t), S^{(-)}(0)\} = -2i\frac{e^{i\omega' t - \gamma t}}{\sin\theta_0}\left[\left(\frac{u_1 v_1}{\Delta}\cos^2\theta_0 + \frac{u_2 v_2}{\Delta}\sin^2\theta_0\right)\sin\omega_0 t + \sin\theta_0\cos\theta_0\cos\omega_0 t\right], \tag{D.12}$$

where $\Delta = u_1 v_2 - u_2 v_1$.

From equations (D.11)–(D.12), we finally obtain the Poisson bracket in the following form

$$\begin{aligned}\{S^{(+)}(t), S^{(-)}(0)\} = -\frac{ie^{-\gamma t}}{4\tilde{\omega}_0(v - \alpha\Omega m_z)}\Bigg\{&\left[((v - \alpha\Omega m_z)m_z + \tilde{\omega}_0)^2 + \frac{1}{4}\alpha^2(1-m_z^2)^2\right]e^{i(\omega'+\omega_0)t} \\ &- \left[((v - \alpha\Omega m_z)m_z - \tilde{\omega}_0)^2 + \frac{1}{4}\alpha^2(1-m_z^2)^2\right]e^{i(\omega'-\omega_0)t}\Bigg\}.\end{aligned} \tag{D.13}$$

Note that each term in the square brackets is manifestly positive. When $\varkappa \to 0$, we have $\tilde{\omega}_0 \to v - \alpha\Omega m_z$, and this equation reduces to Eq. (3.18) in the main text of the paper.